

Collapse of Primordial Clouds II. The Role of Dark Matter

Sandra R. Oliveira, Oswaldo D. Miranda, José C. N. de Araujo
and Reuven Opher

*Instituto Astronômico e Geofísico – Universidade de São Paulo
Av. Miguel Stéfano 4200, São Paulo, 04301-904, SP, Brazil*

ABSTRACT

In this article we extend the study performed in our previous article on the collapse of primordial objects. We here analyze the behavior of the physical parameters for clouds ranging from $10^7 M_\odot$ to $10^{15} M_\odot$. We studied the dynamical evolution of these clouds in two ways: purely baryonic clouds and clouds with non-baryonic dark matter included. We start the calculations at the beginning of the recombination era, following the evolution of the structure until the collapse (that we defined as the time when the density contrast of the baryonic matter is greater than 10^4). We analyze the behavior of the several physical parameters of the clouds (as, e.g., the density contrast and the velocities of the baryonic matter and the dark matter) as a function of time and radial position in the cloud. In this study all physical processes that are relevant to the dynamical evolution of the primordial clouds, as for example photon-drag (due to the cosmic background radiation), hydrogen molecular production, besides the expansion of the Universe, are included in the calculations. In particular we find that the clouds, with dark matter, collapse at higher redshift when we compare the results with the purely baryonic models. As a general result we find that the distribution of the non-baryonic dark matter is more concentrated than the baryonic one. It is important to stress that we do not take into account the putative virialization of the non-baryonic dark matter, we just follow the time and spatial evolution of the cloud solving its hydrodynamical equations. We studied also the role of the cooling-heating processes in the purely baryonic clouds.

Key words: Cosmology: theory – dark matter – early Universe.

1 INTRODUCTION

The models of structure formation consider that all the structures of the Universe, such as galaxies and clusters of galaxies, were formed from the growth of small primordial density fluctuations present, initially, in an homogeneous and isotropic Universe, and that by gravitational instabilities resulted in the structures that we observe today. We are going to see below that we just start the study of formation and evolution of primordial clouds from density perturbations present at the beginning of the recombination era.

The first galaxy formation models that included the effects of gas dissipation were studied by Larson (e.g., 1969, 1974, 1975, 1976). Recently, some authors used hydrodynamics codes including the gas dynamics (e.g., de Araujo 1990, de Araujo & Opher 1988, 1989, 1991, Haiman *et al* 1995, Thoul & Weinberg 1995, Tegmark *et al* 1997, Oliveira *et al* 1998, hereafter paper I, among others) in order to follow the behavior of the baryonic matter and to study the influence of several physical processes on the evolution of the primordial clouds.

Gravity is generally believed to be the dominant force in

the processes of structure formation and the dynamical studies of these systems, based on observational data, reveal that the constituents of the Universe include not only luminous matter, but also a far greater amount of dark matter which influence the luminous matter through its gravitational field. For systems such as galaxies and clusters, hydrodynamical effects are important in the process of their formation and thus, hydrodynamics codes which include dark matter are then the most accurate manner to follow the cosmological evolution of the primordial clouds (see, e.g., Cen *et al* 1990, Cen 1992, Cen *et al* 1993).

On the other hand, there are several non-gravitational processes that are important to the evolution of primordial clouds at high redshift, as the photon-drag due to the cosmic background radiation, the recombination processes and the hydrogen molecular formation. These physical processes are important during and after the recombination era. In general, the models that use hydrodynamical numerical codes, found elsewhere, do not initiate the calculations at the beginning of the recombination era, when the perturbations of the baryonic matter can effectively begin to be significantly amplified, whether they are Jeans unstable, and do

not include the above mentioned physical processes.

In the present article we used the set of hydrodynamic equations of the paper I to analyze the behavior of the physical parameters using first only purely baryonic clouds. We then compare the evolution of the physical parameters including non-baryonic dark matter. We start all the calculations present here at the beginning of the recombination era and take into account all the relevant physical processes present during and after the recombination era, besides the expansion of the Universe.

In §2 we describe the basic equations, in §3 we discuss our results and finally in §4 we present our conclusions.

2 EQUATIONS

We consider spherically symmetric density perturbations which produces clouds of baryonic matter and dark matter with densities greater than the density of the Universe. We consider the baryonic matter and dark matter as two fluids coupled by gravity.

The equations for a purely baryonic matter are described in greater detail in paper I, and so, here we only summarize them, namely:

$$\frac{\partial \rho}{\partial t} + \frac{1}{r^2} \frac{\partial}{\partial r} (r^2 \rho v) = 0 \quad (1)$$

$$\frac{D\vec{v}}{Dt} = -\frac{1}{\rho} \nabla P - \nabla \phi - \frac{\sigma_T b T_r^4 x}{m_p c} \left[\vec{v} - \frac{\dot{R}(t)}{R(t)} \vec{r} \right] \quad (2)$$

$$\frac{DE}{Dt} = \frac{P}{\rho^2} \frac{D\rho}{Dt} - L \quad (3)$$

$$\frac{Dx}{Dt} = C \left\{ \beta e^{-\frac{(B_1 - B_2)}{k T_r}} (1 - x) - \frac{a \rho x^2}{m_p} \right\} + I \quad (4)$$

As in paper I, the Eqs.(1)–(4) are, respectively, the equation of conservation of mass, conservation of momentum, energy and ionization balance. Where ρ is the mass density of the cloud, r is the radial coordinate, v is the velocity. The velocity is written as $\vec{v} = \vec{v}_n + \vec{v}_H$, where \vec{v}_n is the peculiar velocity of the cloud and $\vec{v}_H = H\vec{r}$ (where $H \equiv \dot{R}(t)/R(t)$ is the Hubble parameter, $R(t)$ is the scale factor and $\dot{R}(t)$ its time derivative). The pressure of the cloud is $P = kN\rho T_m(1 + x)$ (where k is the Boltzmann constant, N is the Avogadro's number, T_m is the temperature of the matter, and x is the degree of ionization), σ_T is the Thomson cross section, $b = 4\sigma_{SB}/c$ (where σ_{SB} is the Stefan-Boltzmann constant), T_r is the temperature of the radiation, m_p is the mass of the proton, c is the velocity of light.

The gravitational potential is $\nabla \phi = GM(r)/r^2$, with G the gravitational constant. The term $M(r)$ is the total mass (i.e. the baryonic and non-baryonic dark matter) contained inside the radius r of the cloud. We here take the total amount of baryonic matter and dark matter constant during the evolution of the clouds.

The cooling-heating processes are included in the cooling function L . This term is the summation of four mechanisms; $L = L_R + L_C + L_{H_2} + L_\alpha$. Where, L_R is the cooling due to recombination (see, e.g., Schwarz *et al* 1972), L_C is the

Compton cooling (see, e.g., Peebles 1968), L_{H_2} is the cooling by molecular hydrogen (see, e.g., Lepp & Shull 1983) and L_α is the Lyman- α cooling (see, e.g., Calberg 1981). The temperatures in our calculations are never greater than $\sim 10,000K$ and thus, the cooling-heating mechanisms considered here are the dominant mechanisms for the thermal history of the baryonic matter contained inside the clouds.

In order to consider the *DM* (non-baryonic dark matter) models, we included the following equations:

$$\frac{\partial \rho_{DM}}{\partial t} + \frac{1}{r^2} \frac{\partial}{\partial r} (r^2 \rho_{DM} v) = 0 \quad (5)$$

$$\frac{D\vec{v}_{DM}}{Dt} = -\nabla \phi \quad (6)$$

$$\vec{v}_{DM} = \vec{v}_{n_{DM}} + \vec{v}_H \quad (7)$$

$$\nabla \phi = \frac{GM(r)}{r^2} \quad (8)$$

the various terms appearing in the Eqs.(5)–(8) are analogous to those found in the hydrodynamical equations to the baryonic matter.

We consider that the primordial clouds evolve within a medium of density ρ_u (the density of the Universe) and so we take into account this fact in our study; see paper I to the hydrodynamical equations of the Universe.

The initial perturbation is taken to be in the form of a power law spectrum as considered, for example, by Gott & Rees (1975)

$$\delta_i = \frac{\delta \rho}{\rho} = \left(\frac{M}{M_o} \right)^{-\frac{1}{2} - \frac{n}{6}} (1 + z_{rec})^{-1} \quad (9)$$

with M the mass of the cloud, M_o the reference mass, n the spectral index and z_{rec} the redshift at the beginning of the recombination era. It is important to stress that M is the total mass of the clouds, i.e., $M = M_B + M_{DM}$ (where “ B ” refers to the baryonic matter and the “ DM ” refers to the non-baryonic dark matter). The normalization of the spectrum of perturbations given above was made to agree with the COBE data (see e.g. de Araujo & Opher 1994).

We consider that initially the density profile of the cloud is “top hat” like, and we begin the calculations when the radiation temperature is $\simeq 4,000K$ ($z \simeq 1500$) where the ionization degree begins to be significantly lower than one. We use $\Omega_B = 0.1$ (the baryonic density parameter) and different values for Ω_{DM} (the non-baryonic dark matter density parameter), as well as different values for the Hubble constant, h (the Hubble constant in units of $100 km s^{-1} Mpc^{-1}$). We consider that the clouds initially expand with a field velocity given by the Hubble flow.

We follow the evolution of the cloud until its collapse, that we consider as the time, after the recombination era, when the density contrast of the cloud is greater than 10^4 . We used in our calculations 1,200 spherical shells for the baryonic matter and 1,200 shells for the dark matter. Models with 6,000 shells for both components showed no considerable difference in the results. The complete set of partial

differential equations has been written in the form of difference scheme by one of us (Miranda 1998) according to the basic method described by Richtmyer and Morton (1967).

3 CALCULATIONS AND DISCUSSION

The scale of masses studied ranges from $10^7 M_\odot$ to $10^{15} M_\odot$. We show, in particular, three points in the cloud; the first shell, the middle shell of the scheme, and the last shell as a function of time. In order to analyze the radial behavior, we show five different times for the output of the data: t_i – time at the recombination era, $t_2 = (t_3 - t_i)/2$, $t_3 = (t_f - t_i)/2$, $t_4 = (t_f - t_3)/2$ and t_f , where t_f is the time of the collapse of the core.

Also, as already mentioned in the paper I, due to the expansion of the Universe, even the clouds that are already Jeans unstable and eventually collapse undergo, initially, an expansion phase before collapsing (see paper I for more details).

We divided our paper in two parts. Firstly we studied purely baryonic clouds and we analyzed the behavior of the variables along the evolution of time, and in different points inside the cloud. We also studied the influence of the cooling-heating processes. To do this we studied individually the effects of all the four cooling-heating processes and the photon drag (Tables 2–4). The results are described in subsection 3.1.

Secondly, we included *DM* and analyzed the behavior of the same variables in the same way, except the analysis of the cooling-heating processes. The results of baryonic plus *DM* model are described in subsection 3.2.

3.1 Purely baryonic clouds

We now show the results of the purely baryonic models. We ran our models for masses ranging from $10^7 M_\odot$ to $10^{15} M_\odot$. Here we ran the models with $M_o = 4 \times 10^{17} M_\odot$, $h = 1$, $\Omega = 0.1$ and $n = -1$. The normalization of the spectrum used here is consistent with σ_8 (see, e.g., de Araujo & Opher 1994 for a discussion). We show these results in the Figs.1-6. It is worth mentioning that a spectrum such as $\delta \propto M^{-1/3}$ is consistent with observations for $1 < r/(h^{-1} Mpc) < 100$ (see for example Kashlinsky & Jones 1991).

Let us first have a look at the evolution of the density contrast, in the Fig.1, and also at the evolution of the density, in the Fig.2. We see that masses within the interval $10^7 M_\odot$ to $10^{10} M_\odot$ have a partial collapse, i.e. our collapse criterion is satisfied only to the internal shells. In particular, for the masses $10^7 M_\odot$ to $10^9 M_\odot$ the density contrast has a slightly oscillation in the external shells and, these shells do not reach a density contrast of 10^4 .

We also analyzed the morphological behavior of the density profile (Fig. 3), in order to see how it is modified as a function of time. For the masses ranging from $10^7 M_\odot$ to $10^{10} M_\odot$, the collapse starts in the internal shells, followed by the outermost shells, as discussed above. For the masses greater than $10^{13} M_\odot$, there is no collapse (at least for the normalization of the spectrum of perturbations studied here). Along the radius the initial “top hat” profile changes rapidly with time for masses smaller than $10^{10} M_\odot$. This is related to the fact that masses lower than $10^{10} M_\odot$ have a pressure gradient that modify the initial density profile. This

shows that to assume that the density profile is “top hat” throughout the cloud evolution is not a good assumption, as considered, e.g., by de Araujo & Opher (1989, 1991, 1994). We are going to see later on that under certain circumstances the use of a “top-hat” density profile throughout the calculations, as assumed by de Araujo & Opher, can provide us interesting informations.

Let us now have a look at the temperature, pressure and molecular density formation (Fig.4). These variables fall with time for all masses because of the cooling and the initial expansion of the clouds. But when the cloud collapses, the temperature increases greatly as expected. An analysis of the molecular density versus temperature is shown in Fig.5. It shows that the molecular density increases when the temperature is within the interval $100K < T < 500K$.

As already explained in paper I, the heat conduction and the Bremsstrahlung are not taken into account. It is worth stressing that in our study we do not take, as initial condition, a virialized object as considered by some authors. Our calculations start at the recombination era when the temperature of the baryonic matter inside the perturbation has the same value as that of the radiation. For clouds that collapse at high redshifts, in general, the principal mechanism that acts in the evolution and collapse of the perturbations is the Compton heating-cooling (see results presented in Tables 5-8 in paper I). Thus, during the expansion phase of the perturbations, when the Compton heating-cooling is efficient, the temperature of the baryonic matter inside the perturbation is almost the same temperature of the radiation.

At the redshift collapse of the clouds, the temperature of the matter increases by a factor 4 or 5 in relation to its correspondent value at the turn-around. Thus, depending on the power spectrum and on the mass of the cloud, the shocks and the collapse itself are not able to rise the temperature of the cloud to $10^4 K$ (see, e.g., Table 5 and the discussion in the Paper I).

Certainly, these results are dependent on the particular way in which we define the collapse of our models, that is, we consider that an object collapsed when the density contrast is greater than 10^4 . The results also depend on the thermal history of the clouds (that depends on the physical processes here considered). As a result no strong shocks occur that could eventually heat the clouds to the virial temperature. If we follow the calculations to higher values of density than the established by our collapse criterion, the temperature will rise above the values here obtained. It is possible that to density contrasts higher than 10^5 strong shocks occur and they would probably heat the gas to values of temperature $> 10^4 K$, as a result other physical processes, as e.g. Bremsstrahlung, would be important to the evolution of the clouds.

In Fig.6 we show the evolution, with the time, of the radii of the shells chosen to show the evolution of the clouds. It is possible to see the instant when the turn-around occurs for these shells.

In Table 1 we present a comparison between our results and the results by de Araujo (1990) and de Araujo & Opher (1994) for purely baryonic clouds. In this table we also present calculations using the normalization consistent with $\sigma_8 = 1$ (see, e.g., de Araujo & Opher 1994), thereby we have to use $M_o = 4 \times 10^{17} M_\odot$ in Eq.(9). In fact this

normalization is more realistic since structures as large as $M = 10^{13} M_\odot$ may be formed.

We note that all masses have collapse redshifts similar to those obtained by de Araujo and de Araujo & Opher using both normalizations, this is a very interesting result. If one would like only to have an idea of the collapse epoch, the use of a “top hat” profile throughout all the cloud evolution is a good approximation (see, e.g., de Araujo & Opher 1994).

As mentioned in paper I the clouds stop expanding when $(\delta\bar{\rho}/\rho) > 4.6$, therefore above the linear regime. As seen in paper I, we also obtain in the present calculations that the clouds stop expanding when $(\delta\bar{\rho}/\rho) > 4.6$. This very fact explains why, even in the non-linear regime, some clouds studied here neither collapses nor stops expanding.

It is worth stressing that the collapse redshift calculated here gives us only an idea of the epoch in which the collapse occurs, due to the fact that the formation of a galaxy, for example, is a process much more complex. In fact, what we do, it is a study of formation of a proto-object. The present study is of interest due to the fact that we show how a density perturbation could give rise to a proto-object and also we show which physical processes are important during and after the recombination era.

We now study the influence of the cooling-heating processes on the evolution of clouds taking, as representative examples, clouds with the masses $10^7 M_\odot$, $10^9 M_\odot$ and $10^{11} M_\odot$ (Tables 2–4). To do this, we disregard, one at a time, all of the four cooling-heating processes and also the photon drag. The results are consistent with paper I, i.e., these very physical processes are important on the evolution of the clouds determining, for example, the collapse epoch and the thermal history of the clouds.

The analysis of the cooling mechanisms show that when we disregard the Compton cooling-heating, the collapses occur earlier. This is due to the fact that the Compton mechanism heats the cloud when the temperature of the matter is lower than the temperature of the radiation, in this way during the recombination era the Compton cooling-heating maintains the temperature of the cloud near to the temperature of the cosmic background radiation. Due to the expansion of the Universe the clouds firstly expand and whether the Compton heating was not present the clouds would expand almost adiabatically, as a result their temperatures would get smaller, and so their pressures, thereby the clouds would stop expanding earlier.

When we disregard the photon drag the clouds also collapse earlier. As we show in paper I the photon drag acts distinctly on the smaller masses ($< 10^6 M_\odot$) and on the greater masses. Here it acts against the collapse, as a brake, but its action is not so strong like it was for the smaller masses.

The cooling by molecular hydrogen does not influence the collapse redshift, its influence is on the thermal history of the cloud. The other physical processes here studied have a behavior similar to that described in paper I.

We studied also the behavior of the collapse of the clouds when we change h and Ω . The results are in Tables 5 and 6. As a general conclusion it can be mentioned that the collapse redshift, the maximum mass of the objects formed, and also the thermal history of the clouds depend strongly on h and Ω . When we change, for example, Ω from 0.1 to 0.2 we have collapses occurring earlier. On the other hand, when we change h from 1 to 0.5 we have the collapses

Table 1. The redshifts of collapse

M/M_\odot	$M_o = 4 \times 10^{17} M_\odot$		$M_o = 10^{15} M_\odot$	
	z_c^*	z_c^{A*}	z_c	z_c^A
10^7	437	–	102	108
10^8	238	–	49	49
10^9	153	–	20	21
10^{10}	77	75	6.5	7
10^{11}	34	34	NC	–
10^{12}	12	13	NC	–
10^{13}	2.1	3.6	NC	–

We compare here the redshifts of collapse of the present article (z_c^*), with those by de Araujo (1990) (z_c^A) and de Araujo & Opher (1994) (z_c^{A*}). We use $n = -1$, $h = 1.0$ and $\Omega_B = 0.1$. We studied two normalizations, namely, $M_o = 10^{15} M_\odot$ and $M_o = 4 \times 10^{17} M_\odot$. NC stands for “no collapse”.

occurring latter, as expected.

3.2 Baryonic plus DM clouds

We now discuss the results of our models including the presence of the dark matter. We ran our models for masses ranging from $10^7 M_\odot$ to $10^{15} M_\odot$. Here we ran initially all models with $M_o = 4 \times 10^{17} M_\odot$, $h = 0.5$, $\Omega_B = 0.1$, $\Omega_{DM} = 0.5$ and $n = -1$, and we show these results in the Figs.7–13. In order to compare we also ran models with different combinations of h and Ω_{DM} , as well as, a different normalization of the spectrum of density perturbations.

The behavior of the density is shown in Fig.7 (time evolution) and Fig.8 (spatial evolution). For the normalization of the spectrum of perturbations used here, the maximum mass that collapses is $10^{14} M_\odot$.

It is worth mentioning that the explanation of why there is no collapse for some clouds, as could be expected, is due to the fact, as already mentioned, that it is necessary to have $(\delta\bar{\rho}/\rho) > 4.6$ to the cloud stops expanding and starts its collapse.

We see, from Fig.7, right side, that all masses have partial collapse for the baryonic component, the outermost shells expand with the Universe. For the *DM* component (left side of the Fig.7), this partial collapse occurs only for the cloud of $10^{14} M_\odot$.

In Fig.8 we see that the top hat profile is destroyed as time goes on, particularly to the baryonic matter. In the *DM* component (left side of Fig.8) the top hat profile is maintained almost all the time during its evolution, but it is destroyed rapidly when the collapse is more evolved, in particular for the cases in which we have $M > 10^{12} M_\odot$.

The *DM* profile is maintained due to the fact that it is pressure free, but when the gravitational influence of the baryonic matter, that is no pressure free, begins to be important the top hat profile of the *DM* component is destroyed.

The behavior of the velocity profile is shown in Fig.9 (time evolution) and Fig.10 (spatial evolution). In the baryonic matter component (right side of Fig.10), the profile of the velocity begins linear but it changes rapidly with time, just like in the purely baryonic model. The velocity profile of the *DM* component (left side of Fig.12) is maintained linear almost all the time of the cloud evolution, only for clouds of $M > 10^{12} M_\odot$ there is a slightly modification in such a

Table 2. Values of the variables for $M = 10^7 M_\odot$ for purely baryonic clouds. We used $h = 1.0$, $\Omega_B = 0.1$, $M_o = 10^{15} M_\odot$ and $n = -1$.

Variable	with all processes	without L_R	without L_C	without L_{H_2}	without L_α	without photon drag
z_c	103	103	105	103	103	132
$n_{H_2} (cm^{-3})$	10^2	10^2	1	—	10^2	300
$T(K)$	4×10^2	4×10^2	9×10^3	8×10^3	4×10^2	5×10^2
$\rho (gcm^{-3})$	3×10^{-19}	3×10^{-19}	3×10^{-19}	3×10^{-19}	3×10^{-19}	5×10^{-19}

Table 3. Values of the variables for $M = 10^9 M_\odot$ for purely baryonic clouds. We used $h = 1.0$, $\Omega_B = 0.1$, $M_o = 10^{15} M_\odot$ and $n = -1$.

Variable	with all processes	without L_R	without L_C	without L_{H_2}	without L_α	without photon drag
z_c	20	20	228	20	20	28
$n_{H_2} (cm^{-3})$	3	3	10^{-1}	—	3	1
$T(K)$	5×10^2	5×10^2	4×10^2	1×10^4	6×10^2	5×10^2
$\rho (gcm^{-3})$	3×10^{-21}	3×10^{-21}	3×10^{-21}	3×10^{-21}	3×10^{-21}	5×10^{-21}

Table 4. Values of the variables for $M = 10^{11} M_\odot$ for purely baryonic clouds. We used $h = 1.0$, $\Omega_B = 0.1$, $M_o = 10^{15} M_\odot$ and $n = -1$.

Variable	with all processes	without L_R	without L_C	without L_{H_2}	without L_α	without photon drag
z_c	NC	NC	0.14	NC	NC	2.6
$n_{H_2} (cm^{-3})$	1×10^{-9}	3×10^{-8}	1×10^{-6}	—	3×10^{-8}	3×10^{-5}
$T(K)$	10	50	10	10	50	4×10^2
$\rho (gcm^{-3})$	3×10^{-28}	1×10^{-26}	1×10^{-25}	1×10^{-26}	1×10^{-26}	3×10^{-24}

Table 5. Values of the variables for $h = 1.0$, $\Omega_B = 0.2$, $M_o = 10^{15} M_\odot$ and $n = -1$ for purely baryonic clouds.

M/M_\odot	z_c	$n_{H_2} (cm^{-3})$	$T(K)$	$\rho (gcm^{-3})$
10^7	110	20	4×10^2	3×10^{-20}
10^9	24	1	6×10^2	1×10^{-20}
10^{11}	2	2×10^{-5}	3×10^2	3×10^{-24}

Table 6. Values of the variables for $h = 0.5$, $\Omega_B = 0.1$, $M_o = 10^{15} M_\odot$ and $n = -1$ for purely baryonic clouds.

M/M_\odot	z_c	$n_{H_2} (cm^{-3})$	$T(K)$	$\rho (gcm^{-3})$
10^7	93	300	5×10^2	5×10^{-19}
10^9	18	500	6×10^2	3×10^{-22}
10^{11}	NC	10^{-10}	10	3×10^{-29}

behavior.

The temperature, pressure and molecular density formation of the baryonic matter component is shown in Fig.11. As can be seen in Figs.11-12, the production of the H_2 molecules is efficient for all masses, once reached the temperature, of the baryonic matter, in the range $100K < T < 500K$. Near z_c the H_2 production increases, but for the external shells (long dashed line) it is always low, due to the fact that the density of the cloud is also low in such shells.

In Fig.13 we show the behavior of the radii of the shells for the DM component and for the baryonic matter component (left side and right side of the figure, respectively).

Comparing the two matter distribution it can be seen that the DM matter component is more concentrated than the baryonic matter component.

At this point it is worth stressing that in our calculations we perform a purely hydrodynamical study of the evolution of the clouds, we do not consider that neither the DM nor the baryonic matter undergo, for example, virialization.

Due to the fact that there is no virialization for the DM , and that it is pressure free, it does not either undergo the photon-drag effect, and thus the DM gets more concentrated.

Its well known, and widely accepted, that the spiral galaxies have a halo with at least part of it made of non-baryonic dark matter (see, e.g., Persic & Salucci 1990). In this case the $M_B(r)/M_{DM}(r)$ decreases with increasing r , contrary to the results present here, although we here are very far to have a complete model for a galaxy. Virialization and star formation, for example, will certainly modify strongly the history of the proto-objects here studied. The standard scenario of galaxy formation outlined by, for example, White & Rees (1978) explains what could happen with the relative distribution of dark and baryonic matter. The dark matter forms a halo that collapses, and the gas shock heats to the virial temperature and is pressure supported. The gas pressure then decreases through radiative cooling and then sinks leaving behind a halo of dark matter.

In elliptical galaxies the distribution of dark matter is

not well determined as in the spiral galaxies. Based on the X-ray observations of hot gas of ellipticals, probably the best source of information in this case, some authors argued that $M_{BDM} \sim r$ (where BDM is the baryonic dark matter), just like in the spiral galaxies. It is worth stressing, however, that these studies assume that the hot gas is isothermal, but usually the temperature profile is poorly known (see, e.g., Carr 1994). Whether the non-baryonic dark matter and the baryonic dark matter have the same distribution, and whether the ellipticals follow the same DM distribution followed by the spirals, again there is no accordance between our results and the distribution of DM inferred for the ellipticals. On the other hand, we can argue that we are very far to have a complete model for an elliptical galaxy, to justify the lack of accordance.

From X-ray observations it was shown that the cluster of galaxies A665, for example, presents a high concentration of (baryonic) dark matter at its center (see, e.g., Hughes & Tanaka 1992). Similar high concentration of dark matter at the center of clusters was derived for the Perseus (Eyles 1992) and Coma (Briel, Henry & Bohringer 1992) among other clusters. Some authors argued that this dark matter should be dissipative and therefore baryonic, but it could well be, at least part of it, of non-baryonic nature. In this case the non-baryonic dark matter to baryonic matter distribution found in our study for structures with $M > 10^{14} M_\odot$ would be in accordance with the distribution of DM inferred from the X-ray observations of clusters of galaxies, whether the non-baryonic dark matter follows a distribution similar to that followed by the baryonic dark matter.

We also ran models with other combinations of the parameters n , h , Ω_{DM} and M_o to see how, for example, z_c and the maximum mass that collapses are modified. We show these results in Tables 7–9.

In Table 7 we show the collapse redshift, z_c , for $h = 1$ and 0.5 for the normalization $M_o = 4 \times 10^{17} M_\odot$, as well as for the normalization $M_o = 10^{15} M_\odot$. For these cases we assume a Universe with $\Omega_B = 0.1$ and $\Omega_{DM} = 0.5$.

For the normalization $M_o = 4 \times 10^{17} M_\odot$ we obtain no significant differences for z_c when we change $h = 1$ to 0.5. Also, the maximum mass for both cases is $M_{max} = 10^{14} M_\odot$.

For the normalization $M_o = 10^{15} M_\odot$ we also obtain no significant differences for z_c when we change $h = 1$ to 0.5, for all clouds.

Comparing now the results for the two normalizations, we obtain that the values of z_c are higher for $M_o = 4 \times 10^{17} M_\odot$. These results can be understood due to the fact that the normalization $M_o = 4 \times 10^{17} M_\odot$ have a greater initial density contrast when we compare with $M_o = 10^{15} M_\odot$ and thus, for the same values of h and Ω , the normalization $M_o = 4 \times 10^{17} M_\odot$ produces collapse of the clouds before those with the normalization $M_o = 10^{15} M_\odot$.

In Table 8 we compare our purely baryonic models and our baryonic plus DM models with the models by de Araujo & Opher (1991, 1994). For the purely baryonic cases, and in particular for the range of masses studied, there is no significant difference between the results for z_c present here as compared with de Araujo & Opher's results. For the cases with non-baryonic dark matter we obtain values for z_c larger than that obtained by de Araujo & Opher. Comparing now only the results of our studies, we obtain that the inclusion of dark matter makes the collapses to occur earlier.

Table 7. Models with baryonic plus dark matter

M/M_\odot	$M_o = 4 \times 10^{17} M_\odot$		$M_o = 10^{15} M_\odot$	
	z_c ($h = 0.5$)	z_c ($h = 1$)	z_c ($h = 0.5$)	z_c ($h = 1$)
10^7	515	518	131	132
10^8	332	335	66	67
10^9	191	193	31	32
10^{10}	100	101	14	14
10^{11}	49	50	5.7	5.7
10^{12}	22	23	1.6	1.6
10^{13}	9.4	9.5	NC	NC
10^{14}	2.5	2.2	NC	NC
10^{15}	NC	NC	NC	NC

Collapse redshifts of baryonic plus DM models with $\Omega_B = 0.1$, $\Omega_{DM} = 0.5$ and $n = -1$.

Table 8. Collapse redshifts of the models

M/M_\odot	only	baryonic	baryonic plus DM	
	z_{c_B}	$z_{c_{94}}$	$z_{c_{DM}}$	$z_{c_{91}}$
10^7	102	108	132	113
10^8	49	49	67	56
10^9	20	21	32	–
10^{10}	6.5	7	14	–
10^{11}	NC	NC	NC	NC

Comparison of the collapse redshifts of only baryonic models (z_{c_B}), baryonic plus DM models ($z_{c_{DM}}$) and de Araujo & Opher's (1991, 1994) ($z_{c_{91}}$ and $z_{c_{94}}$) models with $M_o = 10^{15} M_\odot$, $n = -1$, $h = 1$, $\Omega_B = 0.1$, $\Omega_{DM} = 0.5$.

Table 9. Comparison of the collapse redshifts of baryonic plus DM models with $M_o = 4 \times 10^{17} M_\odot$, $h = 0.5$ and $\Omega_B = 0.1$.

M/M_\odot	$n = -1$ ($\Omega_{DM} = 0.5$)	$n = -1$ ($\Omega_{DM} = 0.8$)	$n = +1$ ($\Omega_{DM} = 0.5$)
10^7	515	520	1471
10^8	332	336	1435
10^9	191	194	1366
10^{10}	100	102	1235
10^{11}	49	50	997
10^{12}	22	23	635
10^{13}	9.4	9.9	270
10^{14}	2.5	2.8	77
10^{15}	NC	NC	14

From Table 9 we compare the results of the models when we change the slope of the spectrum (n) and the DM content (Ω_{DM}). Comparing the values of z_c when we use $\Omega_{DM} = 0.8$, instead of $\Omega_{DM} = 0.5$, we obtain no significant differences in the results. Also, the maximum mass in both cases is $M_{max} = 10^{14} M_\odot$. Comparing now z_c , for $\Omega_{DM} = 0.5$, with $n = -1$ and $n = +1$ we obtain very different values. The z_c values are very high for all masses studied when we adopt $n = +1$; in fact a power spectrum with such a spectral index produces excessive power. We have for this case collapses of masses of up to $M_{max} = 10^{15} M_\odot$.

4 CONCLUSIONS

In the present investigation, we studied the evolution of density perturbations with the masses ranging from $10^7 - 10^{15} M_\odot$, taking into account a series of physical processes which are present during and after the recombination era. In order to perform such a study, a spherical Lagrangian hydrodynamical code was written, which made possible to follow the spatial and time evolution of the density perturbations with purely baryonic and baryonic plus non baryonic dark matter clouds.

Our main conclusions for purely baryonic models are the following:

- a) Clouds with masses that range from $10^7 - 10^{10} M_\odot$ have a partial collapse, for $M_o = 10^{15} M_\odot$;
- b) Clouds having masses $> 10^{13} M_\odot$ do not have enough time to collapse, for $M_o = 10^{15} M_\odot$;
- c) If one changes the perturbation spectrum we have collapse for masses up to $10^{13} M_\odot$;
- d) The Compton cooling-heating plays a key role in the collapse of the clouds;
- e) the photon-drag delays the collapse and
- f) The H_2 molecules are, in general, very important to the thermal history of the cloud.

Our main conclusion for the baryonic plus DM models are the following:

- a) We have earlier collapse redshifts always, as compared with the purely baryonic models, independent of the combination of the values of n , h , Ω_{DM} and M_o that we used;
- b) In the collapse of the DM the cooling-heating mechanisms and the photon drag, which are very important for the collapse of the baryonic matter, cannot directly alter the collapse of this component and thus the non-baryonic matter is rapidly concentrated in the innermost region of the clouds;
- c) The observations suggest that in clusters of galaxies the dark matter is more concentrated than the baryonic matter. This result is in agreement with our results if the dark matter is of non-baryonic origin.

ACKNOWLEDGEMENTS

We ran the models on a HP-Apollo 9000 (purchased by the Brazilian agency FAPESP) and on the CRAYs EL98 and J90 (CCE/USP).

We thank the referee, Dr. David Weinberg, for helpful comments and suggestions that greatly improved the present version of our paper.

We thank the Brazilian agencies CAPES (SRO) and CNPq (ODM, JCNA and RO) for support.

REFERENCES

- Briel U.G., Henry J.P., Bohringer H., 1992, A&A, 259, L31
 Carr B., 1994, ARA&A, 32, 531
 Calberg R.G., 1981, MNRAS, 197, 1021
 Cen R.Y., Jameson A., Liu F., Ostriker J.P., 1990, ApJ, 362, L41
 Cen R.Y., 1992, ApJ, ApJS, 78, 341
 Cen R.Y., Ostriker J.P., Peebles P.J.E., 1993, ApJ, 415, 423
 Coles P., Lucchin F. 1995, Cosmology. The Origin and Evolution of Cosmic Structure, John Wiley & Sons, New York

- de Araujo J.C.N., 1990, PhD thesis, AGA-120, IAG-USP
 de Araujo J.C.N., Opher R., 1988, MNRAS, 231, 923
 de Araujo J.C.N., Opher R., 1989, MNRAS, 239, 371
 de Araujo J.C.N., Opher R., 1991, ApJ, 379, 461
 de Araujo J.C.N., Opher R., 1994, ApJ 437, 556
 Eyles C.J., Watt M.P., Bertram D., Church M.J., Ponman T.J., Skinner G.K., Willmore A.P., 1991, ApJ, 376, 23
 Gott III R., Rees M.J., 1975, A&A, 45, 365
 Haiman Z., Thoul A.A., Loeb A., 1996, ApJ, 464, 523
 Hughes J.P., Tanaka Y., 1992, ApJ, 398, 62
 Kashilinsky A., Jones B.J.T., 1991, Nature, 349, 753
 Larson R.B., 1969, MNRAS, 145, 405
 Larson R.B., 1974, MNRAS, 166, 585
 Larson R.B., 1975, MNRAS, 173, 671
 Larson R.B., 1976, MNRAS, 176, 31
 Lepp S., Shull J.M., 1983, ApJ, 270, 578
 Miranda O.D., 1998 in preparation
 Oliveira S.R., Miranda O.D., de Araujo J.C.N., Opher, R., 1998, MNRAS (submitted) - Paper I
 Peebles P.J.E., 1968, ApJ, 153, 1
 Peebles P.J.E., 1993, Principles of Physical Cosmology, Princeton UP, Princeton
 Persic M., Salucci P., 1990, ApJ, 355, 44
 Richtmyer R.D., Morton K.W., 1967, Difference Methods for Initial Value Problems, Interscience Pub., New York
 Schwartz J., MacCray R., Stein R.F., 1972, ApJ, 175, 673
 Tegmark M., Silk J., Rees M.J., Blanchard A., Abel T., Palla P., 1997, ApJ 474, 1
 Thoul A.A., Weinberg D., 1995, ApJ, 442, 480
 White S.D., Rees M.J., 1978, MNRAS, 183, 341

FIGURE CAPTIONS

Fig.1 –The evolution of the density contrast (δ) with time for the mass perturbations in the range $10^7 - 10^{12} M_\odot$. The solid line is the internal shell, the short dashed line is the middle shell and the long dashed line is the external shell, where the time is given in years. The input parameters of the models are: $M_o = 4 \times 10^{17} M_\odot$, $h = 1.0$, $\Omega_B = 0.1$ and $n = -1$.

Fig.2 –The evolution of the mass density ρ (in $g\ cm^{-3}$) for the baryonic matter with time. The captions and input parameters for the curves are the same as the Fig.1.

Fig.3 –The mass density ρ versus radius (in pc) of the clouds. The solid line is the initial time (t_i), the short dashed line, long dashed line and very long dashed line are intermediate times (respectively t_2 , t_3 and t_4) and the dashed-pointed line is the final time (t_f). The input parameters are the same as the Fig.1.

Fig.4 –The evolution of the temperature (T in K), pressure of the gas (P in $dyn\ cm^{-2}$) and density of molecules (n_{H_2} in $molecules\ cm^{-3}$). The captions and input parameters for the curves are the same as the Fig.1.

Fig.5 –The evolution of the density of molecules (n_{H_2}) versus temperature (T). The captions and input parameters for the curves are the same as the Fig.1.

Fig.6 –The evolution of the radii of the purely baryonic clouds for $10^7 - 10^{12} M_\odot$ as a function of time. The solid line is the internal shell, the short dashed line is the middle shell and the long dashed line is the external shell, where the time is given in years. The input parameters for these models are

the same as the Fig.1.

Fig.7 –The evolution of the mass density (ρ) with time. The solid line is the internal shell, the short dashed line is the middle shell and the long dashed line is the external shell, where the time is given in years. The input parameters for these models are: $M_o = 4 \times 10^{17} M_\odot$, $h = 0.5$, $\Omega_B = 0.1$, $\Omega_{DM} = 0.5$ and $n = -1$.

Fig.8 –The mass density (ρ) versus the radii of the clouds. The solid line is the initial time (t_i), the short dashed line, long dashed line and very long dashed line are intermediate times (respectively t_2 , t_3 and t_4) and the dashed-pointed line is the final time (t_f). The input parameters are the same as the Fig.7.

Fig.9 –The evolution of the velocity (in $km\ s^{-1}$) with time. The captions and input parameters for the curves are the same as the Fig.7.

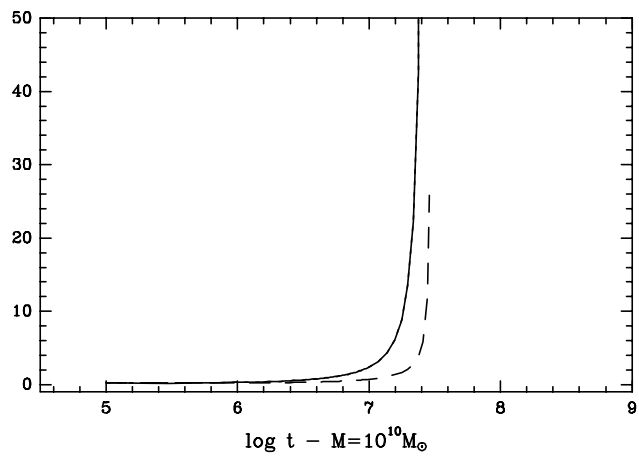
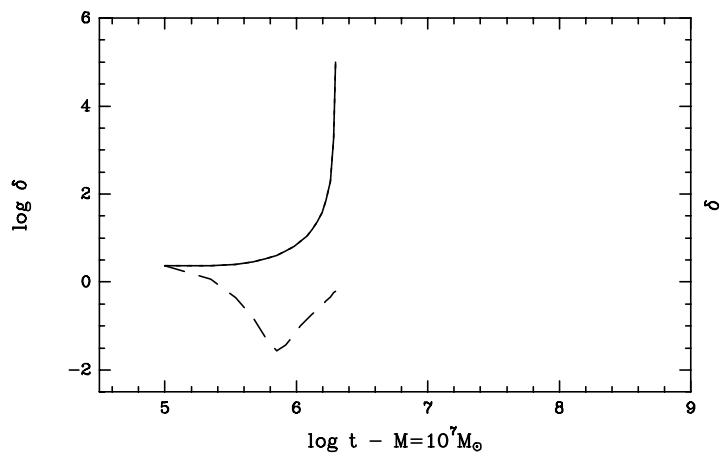
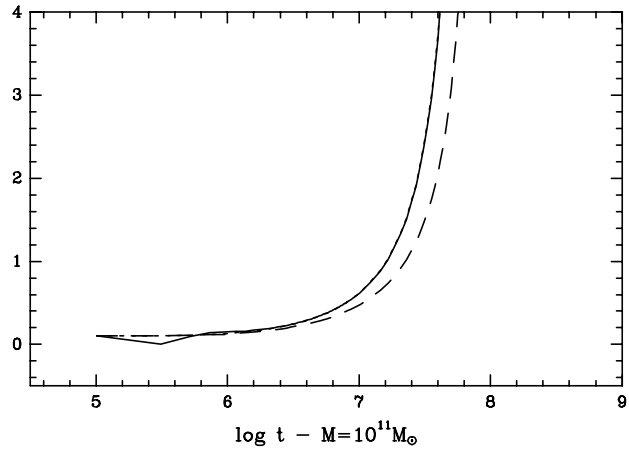
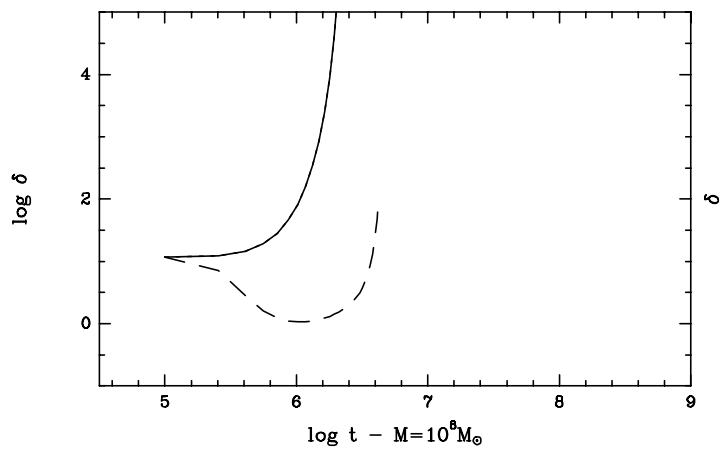
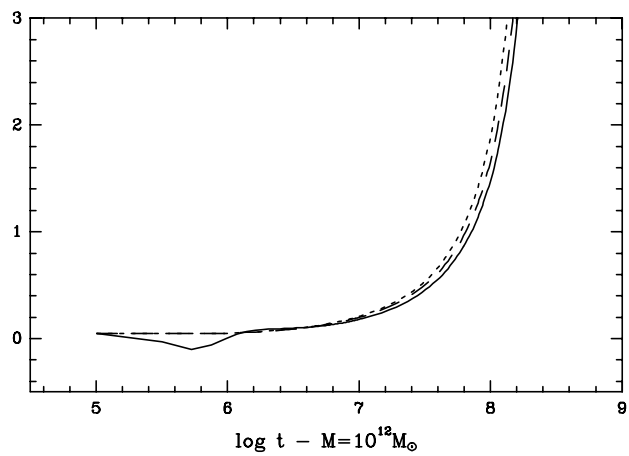
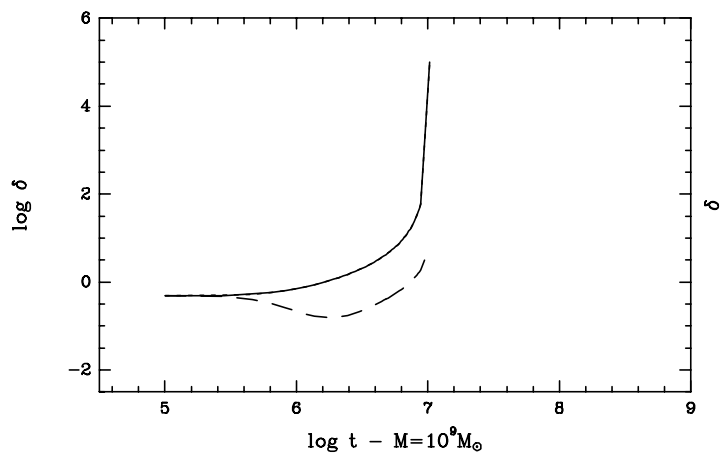
Fig.10 –The velocity profiles to the baryonic and dark matter components. The captions for the curves are the same as the Fig.8. The input parameters for the models are: $M_o = 4 \times 10^{17} M_\odot$, $h = 0.5$, $\Omega_{BR} = 0.1$, $\Omega_{DM} = 0.5$ and $n = -1$.

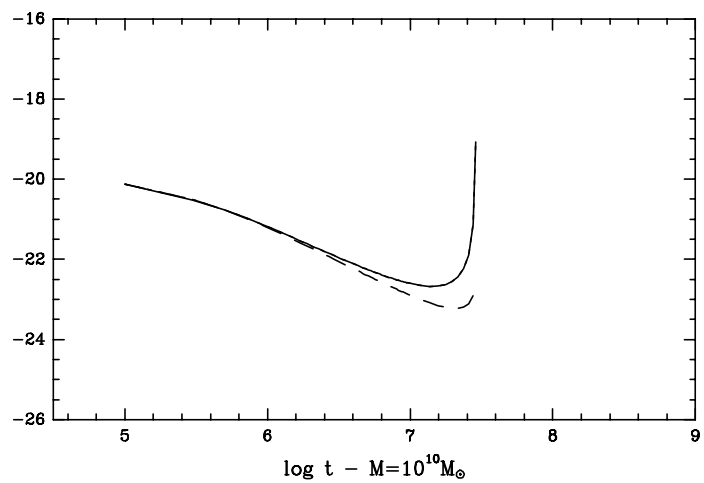
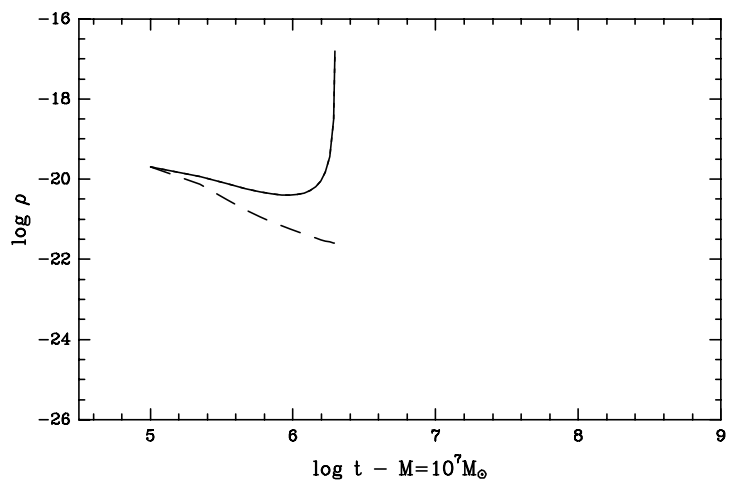
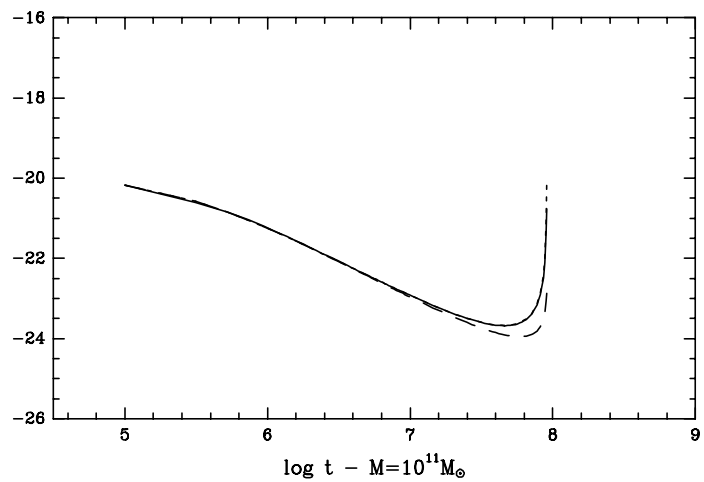
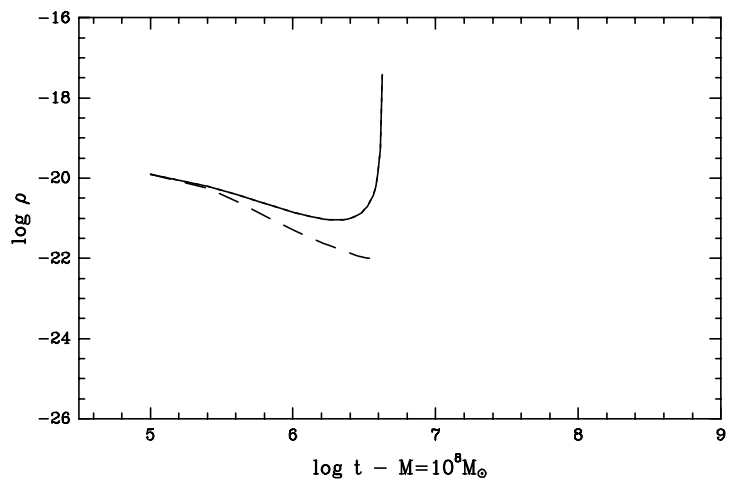
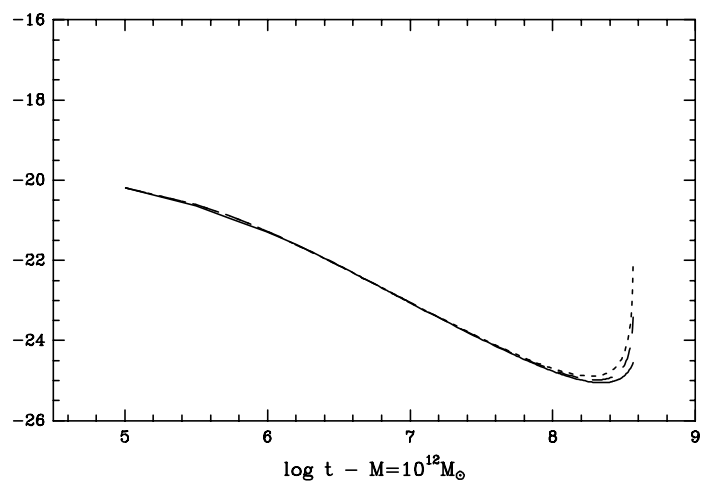
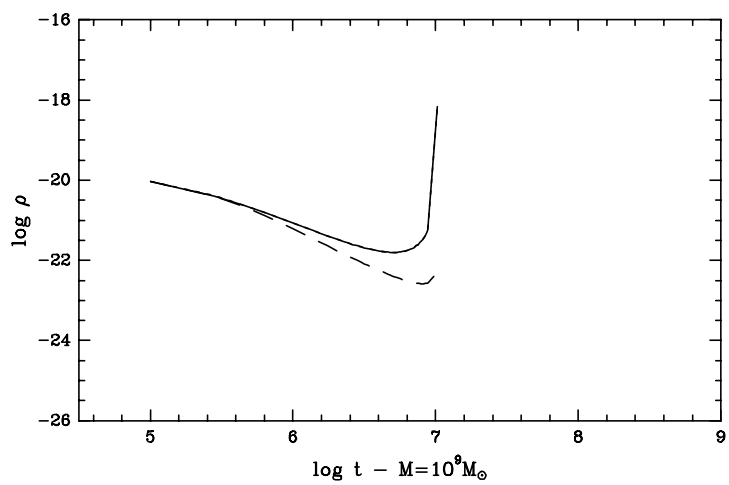
Fig.11 –The evolution of the temperature (T), pressure (P) and density of molecules (n_{H_2}) with time of the baryonic matter component. The captions and input parameters for the curves are the same as the Fig.7.

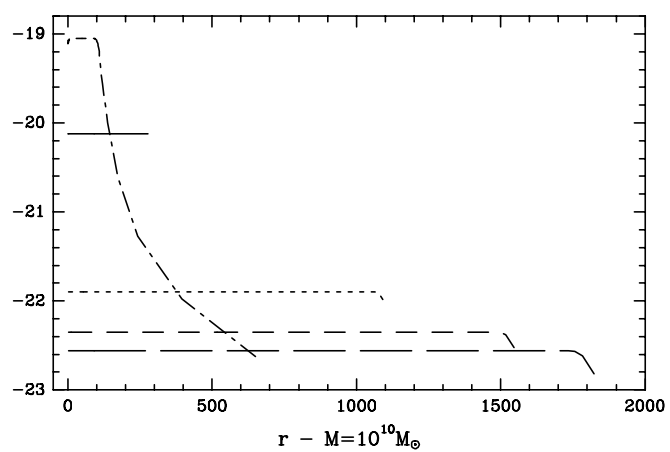
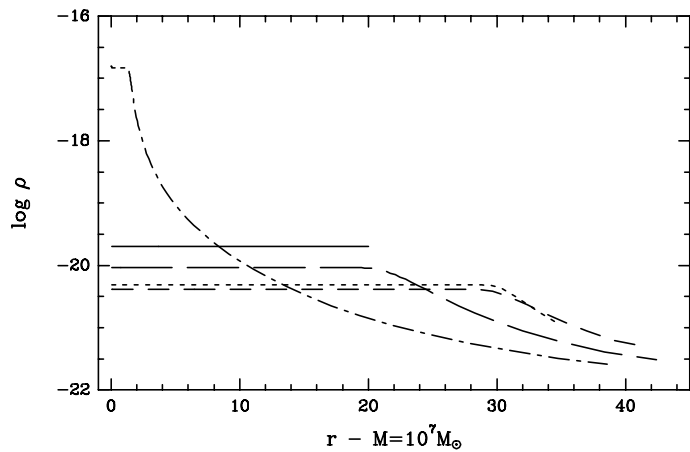
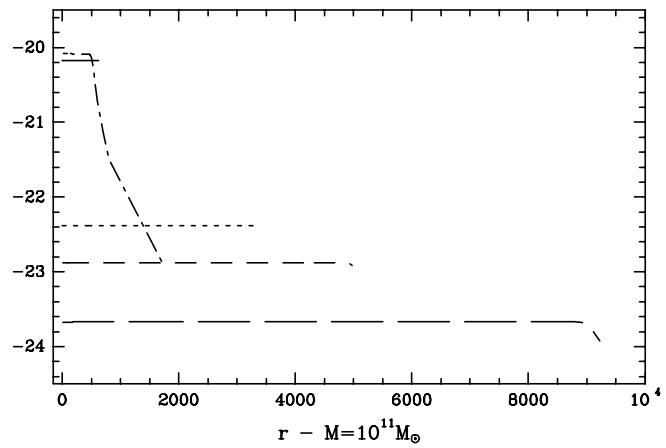
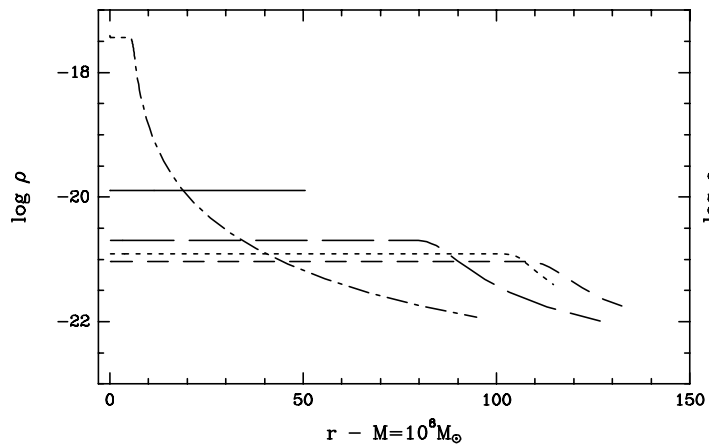
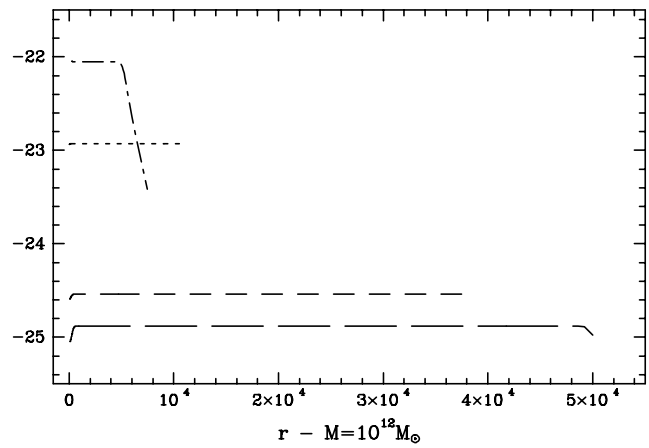
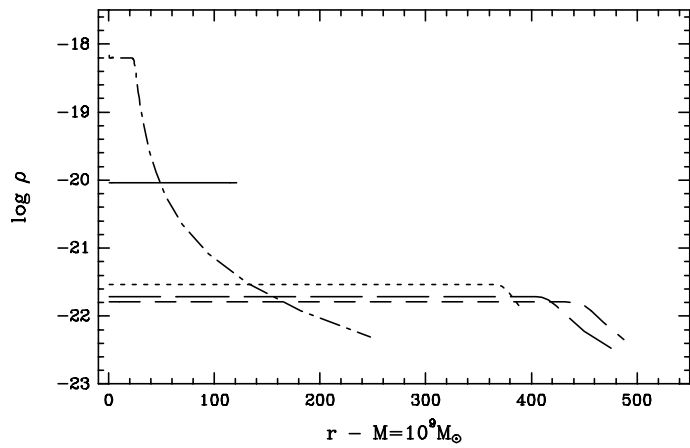
Fig.12 –The temperature of the gas (T) versus the molecular density (n_{H_2}). The captions and input parameters for the curves are the same as the Fig.7.

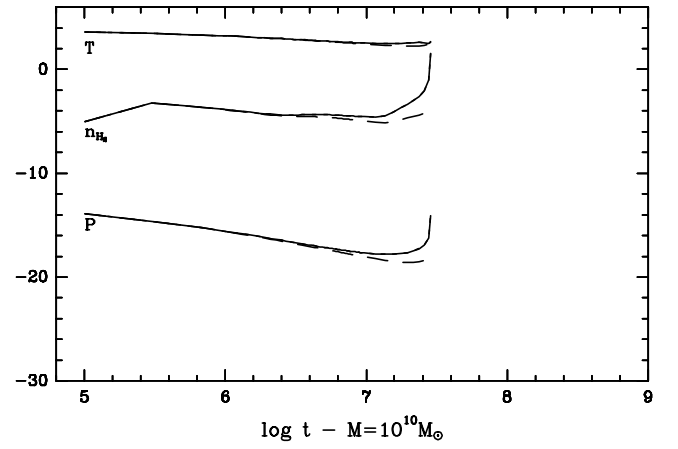
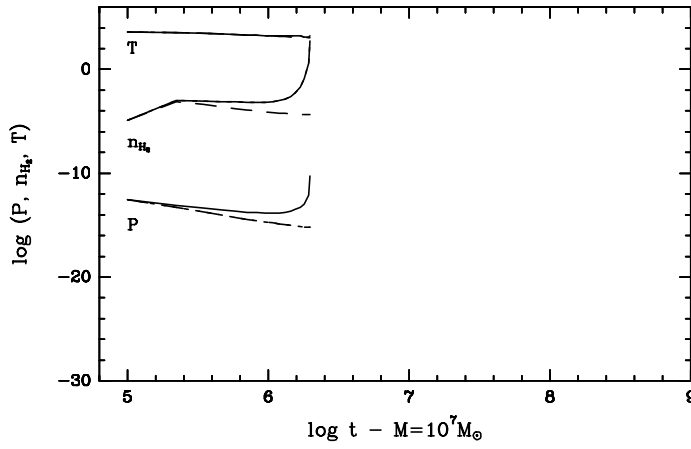
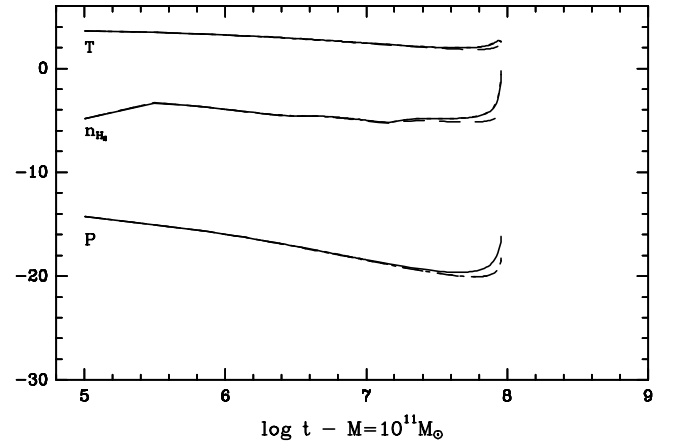
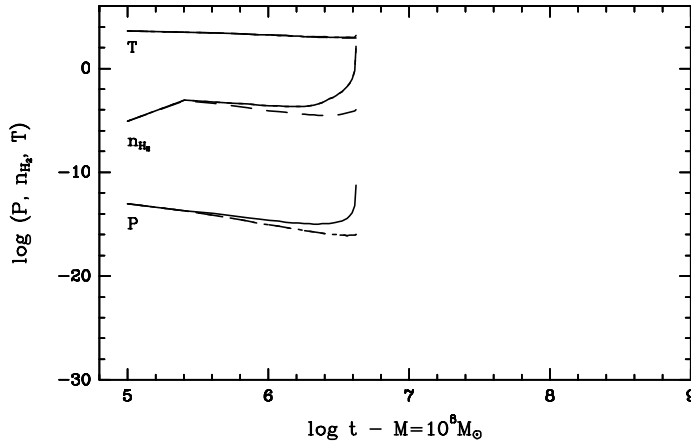
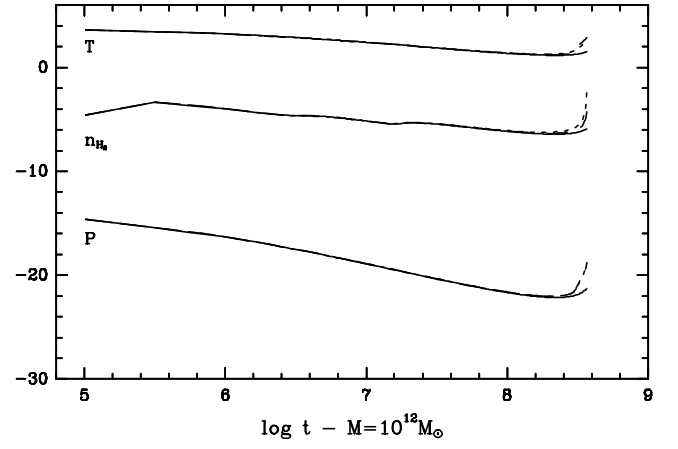
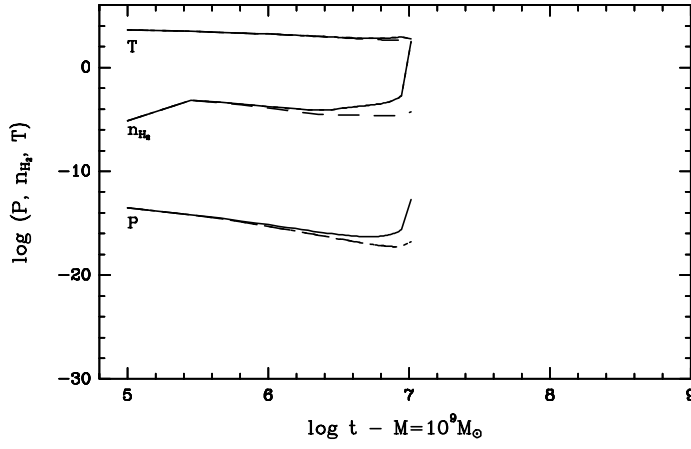
Fig.13 –The evolution of the radius of the baryonic and dark matter components of the clouds with time. The captions and input parameters for the curves are the same as the Fig.7.

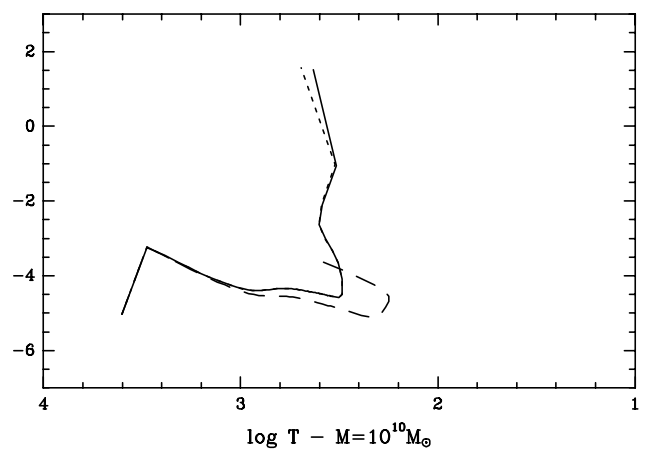
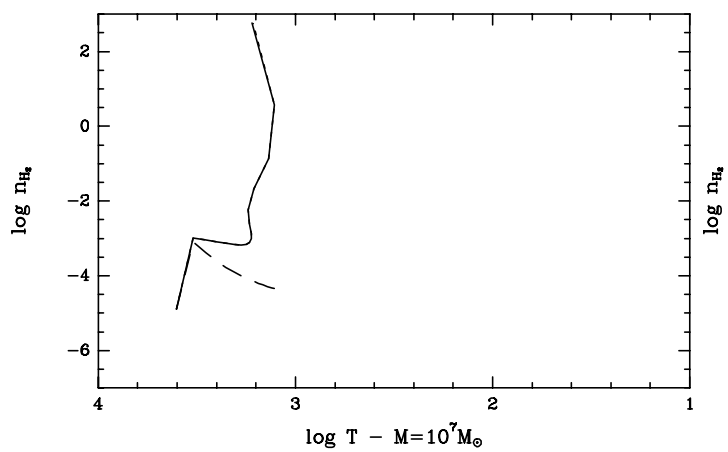
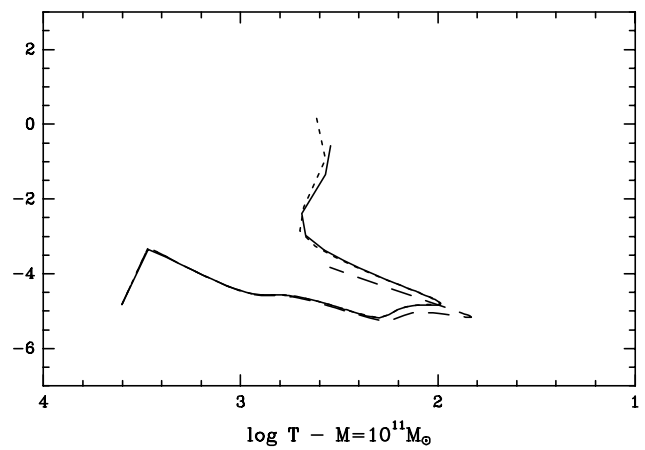
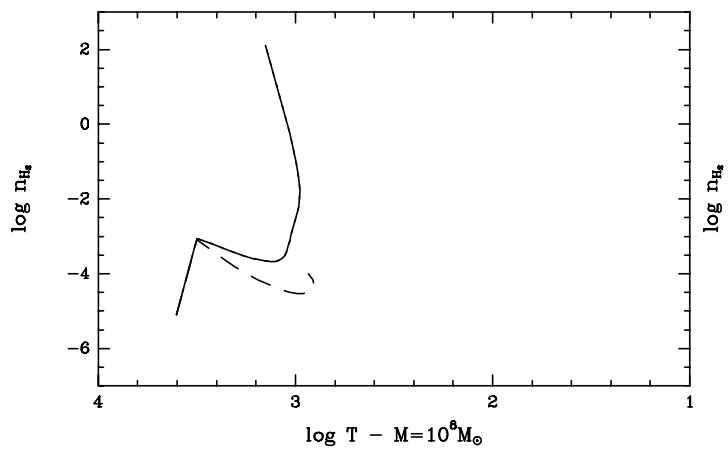
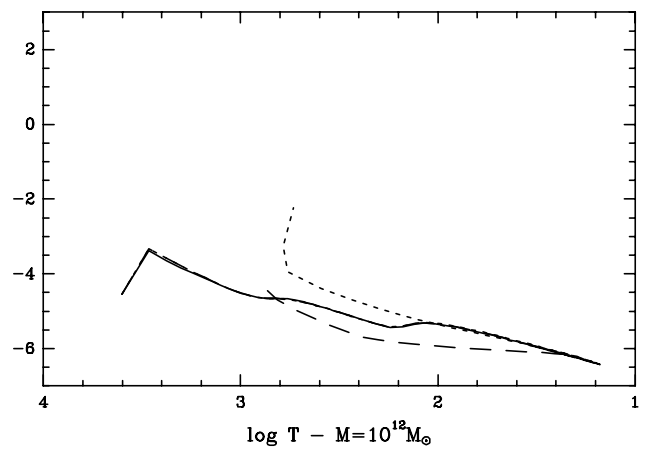
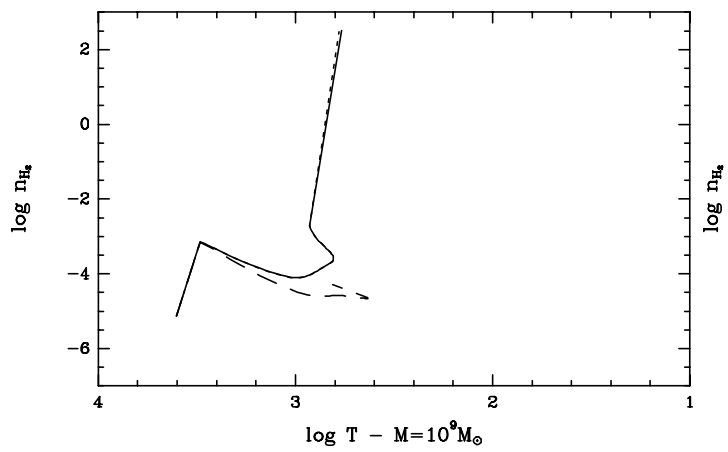
This paper has been produced using the Royal Astronomical Society/Blackwell Science \LaTeX macros.

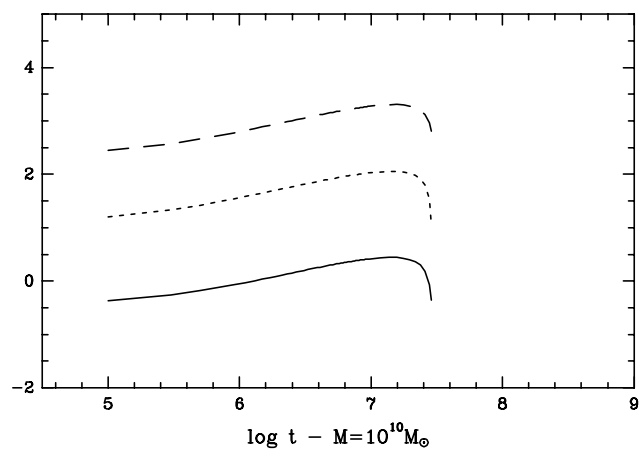
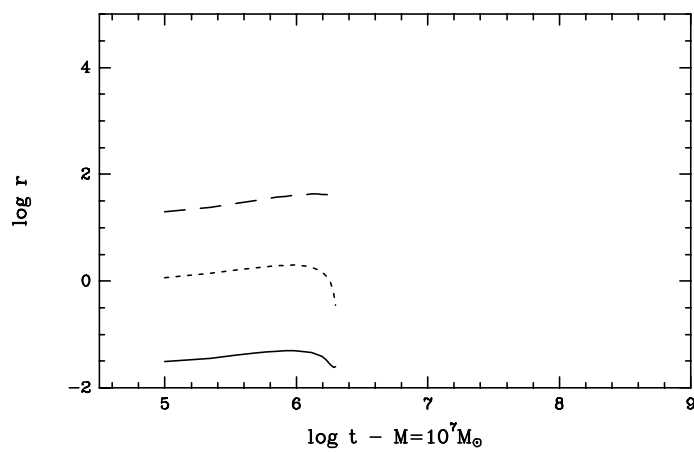
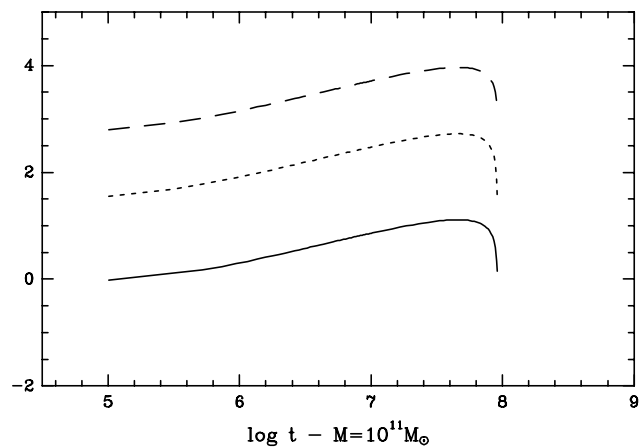
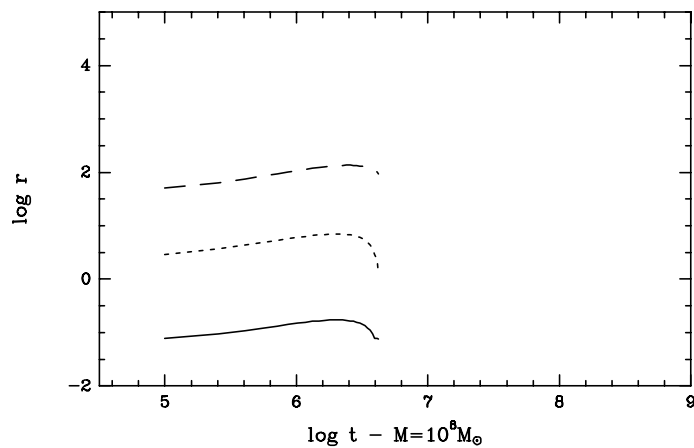
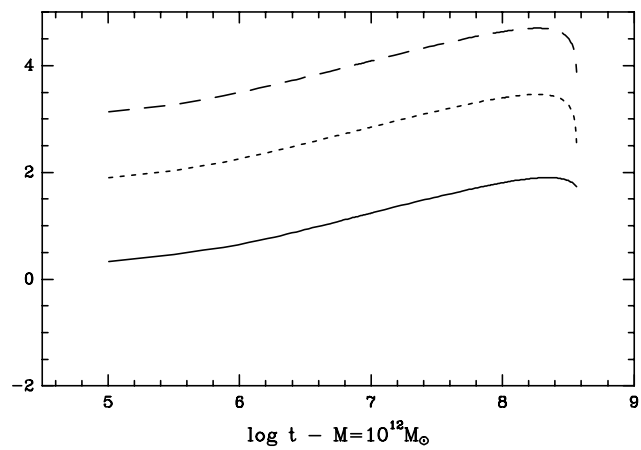
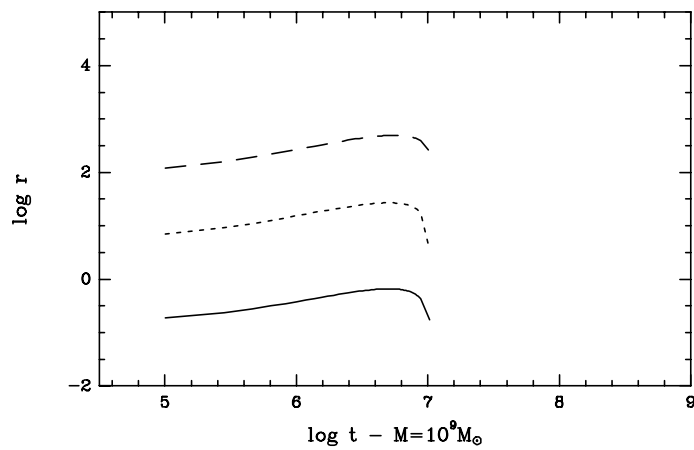




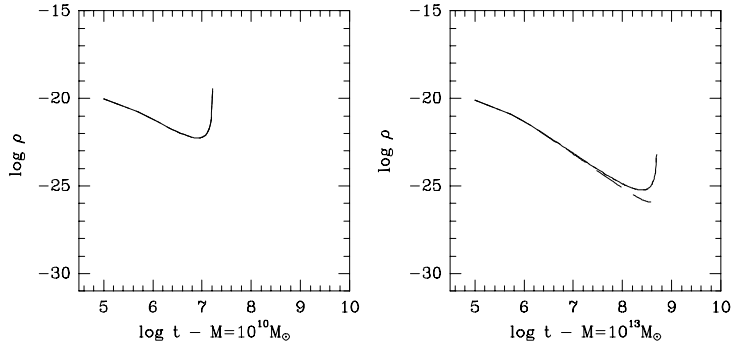




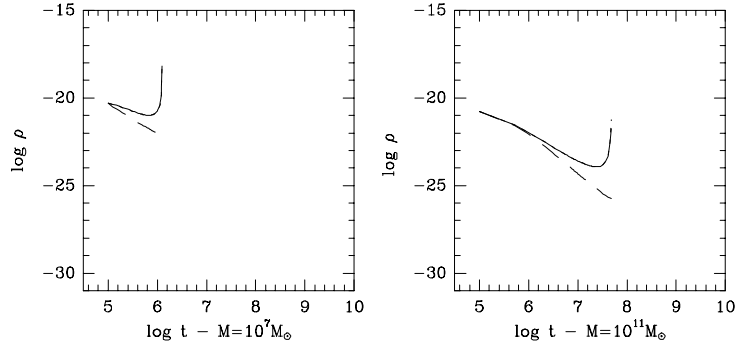
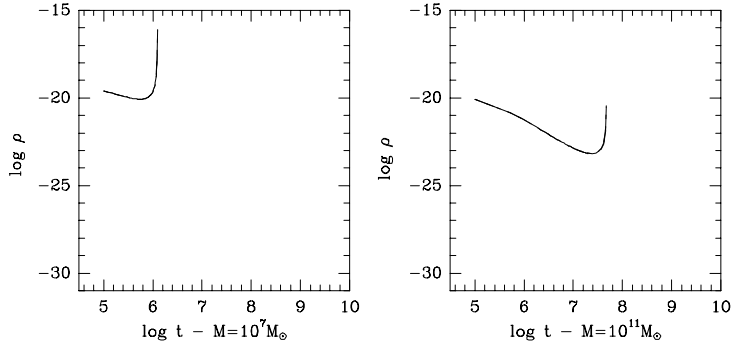
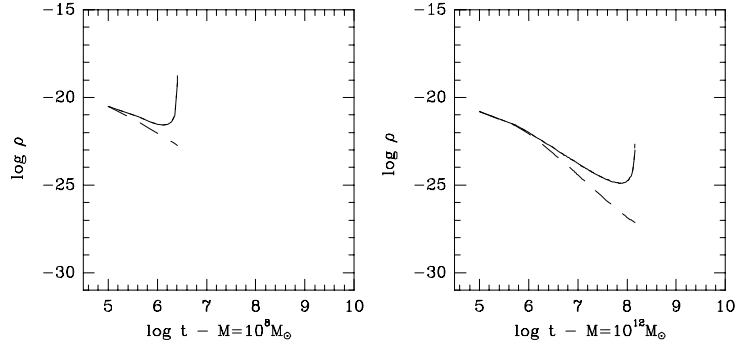
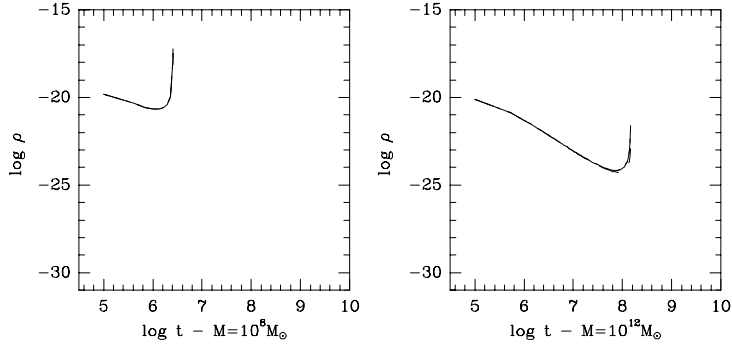
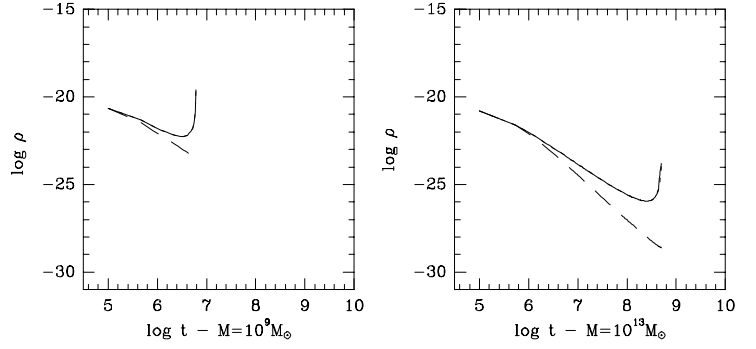
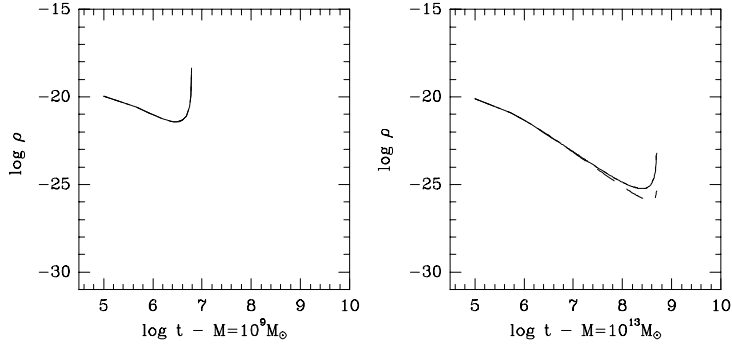
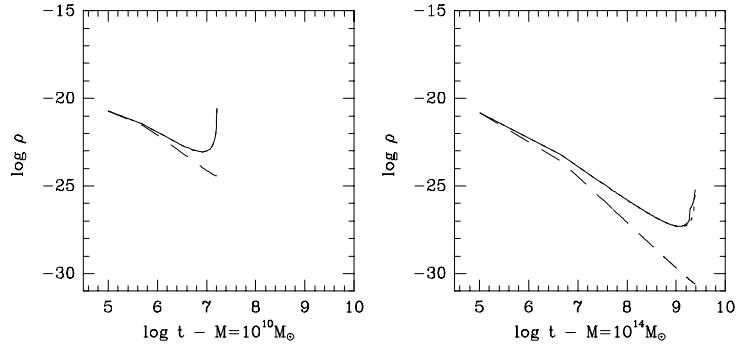




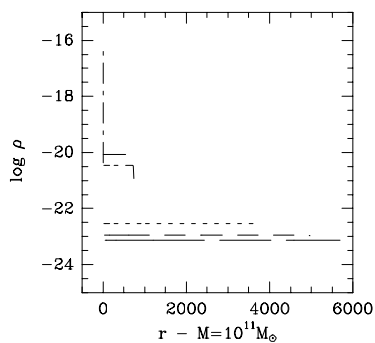
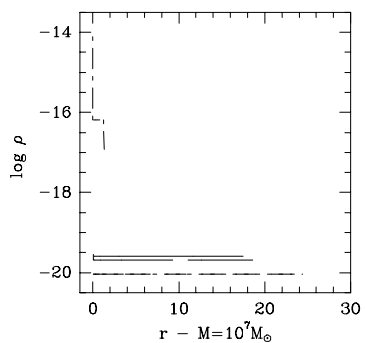
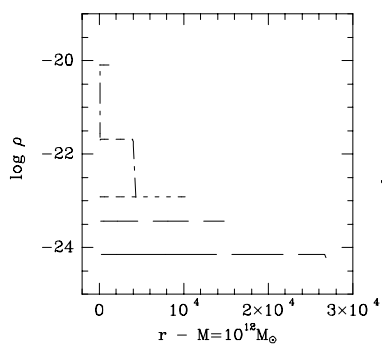
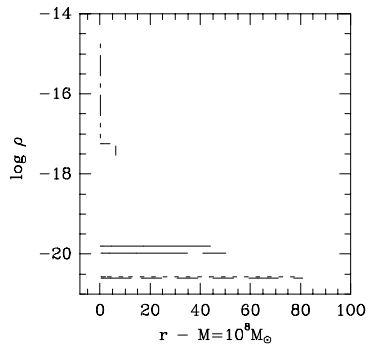
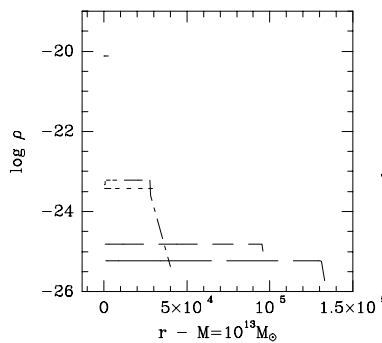
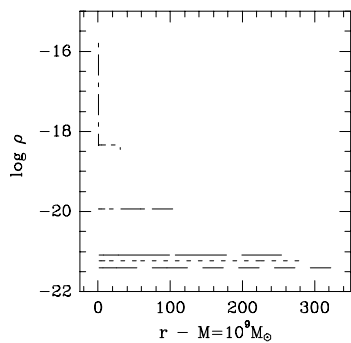
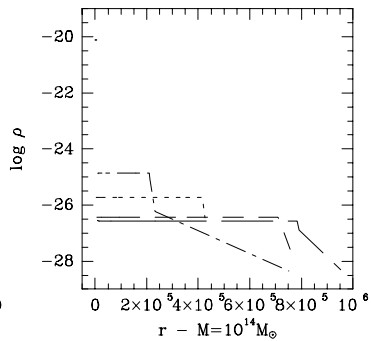
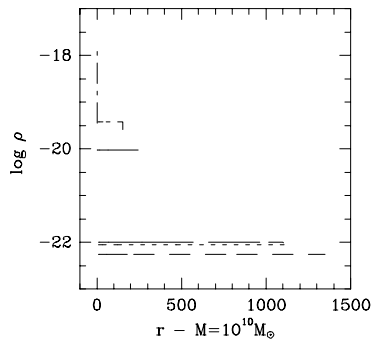
DARK MATTER



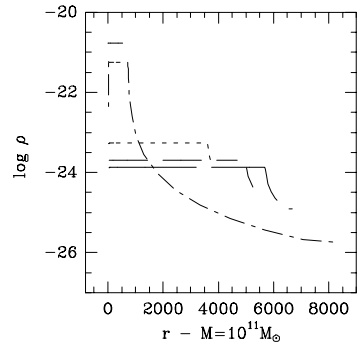
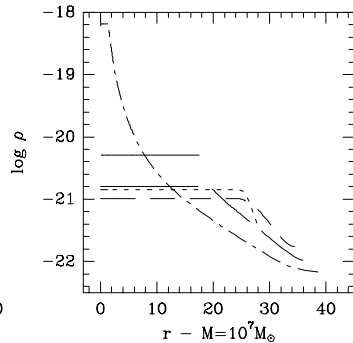
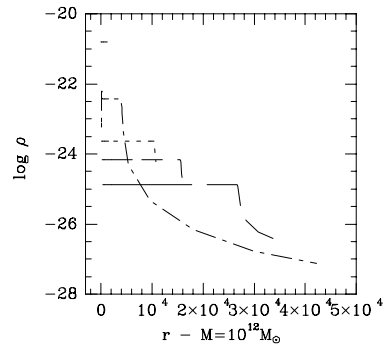
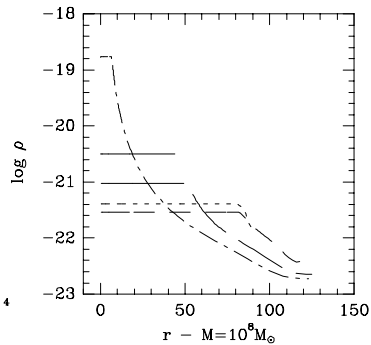
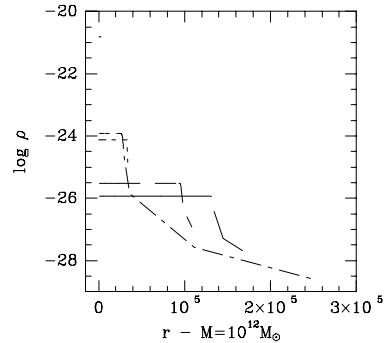
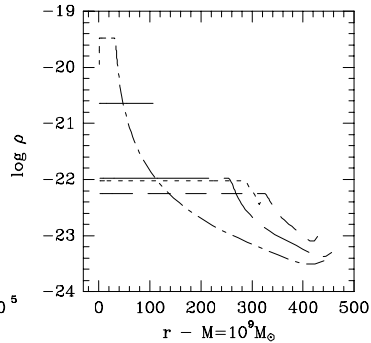
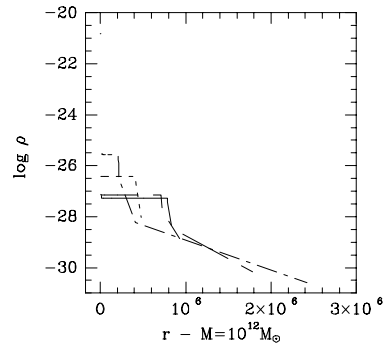
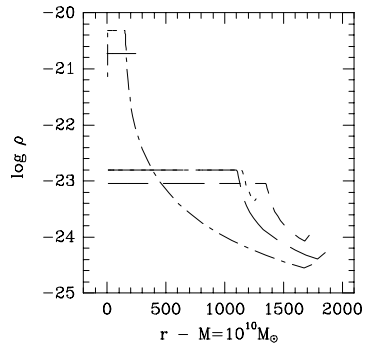
BARYONIC MATTER



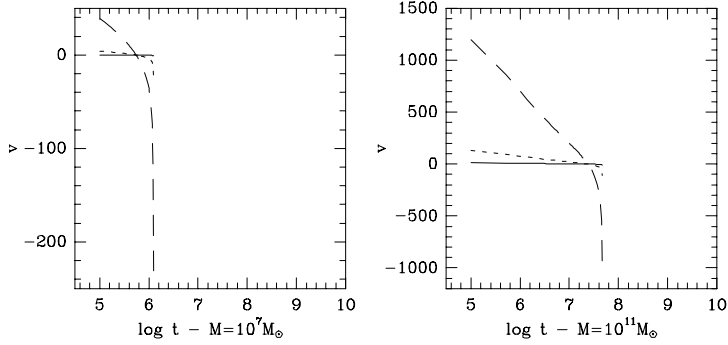
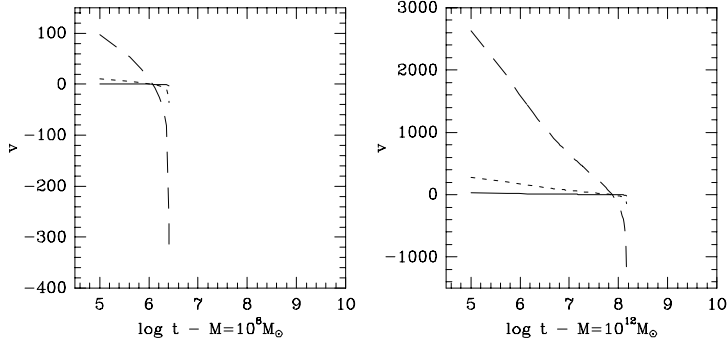
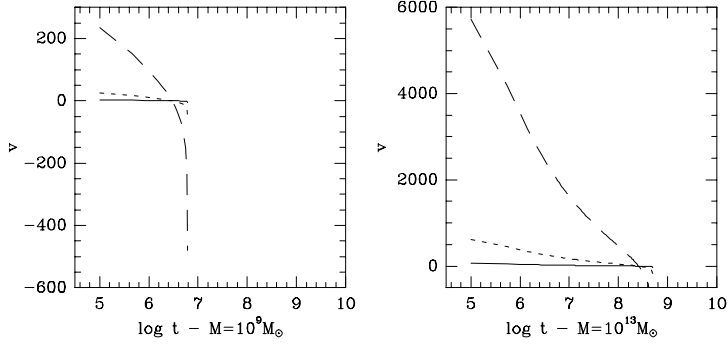
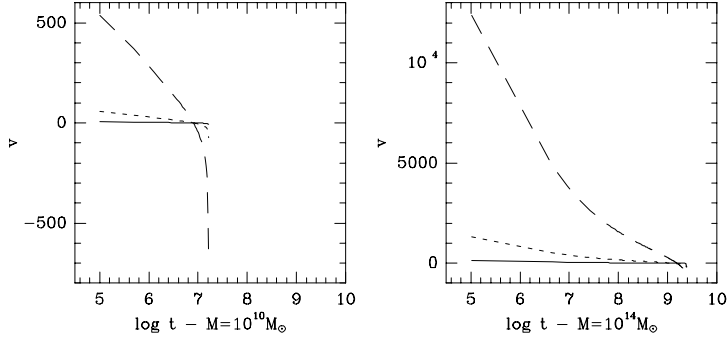
DARK MATTER



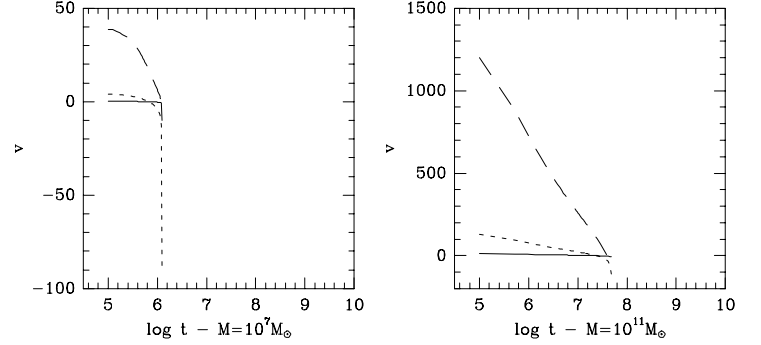
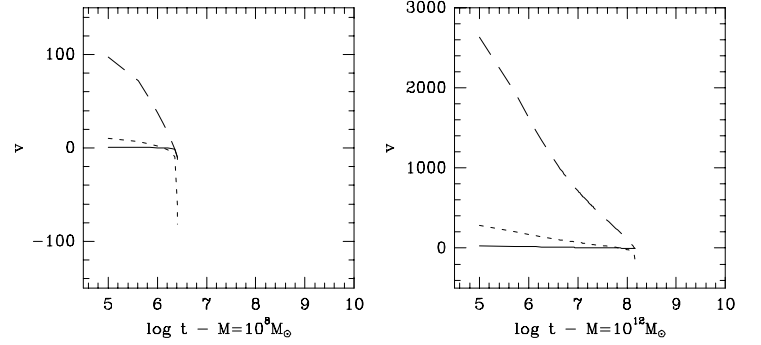
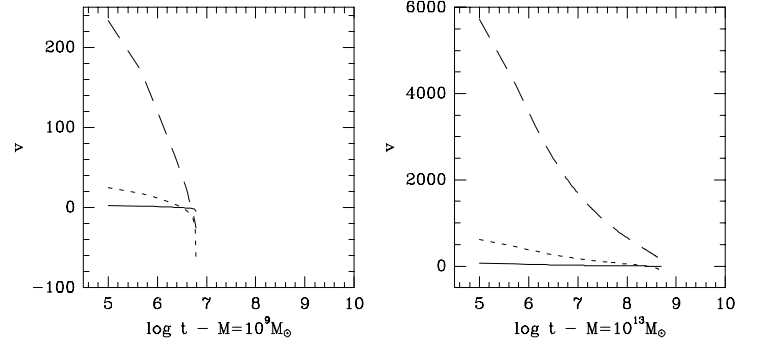
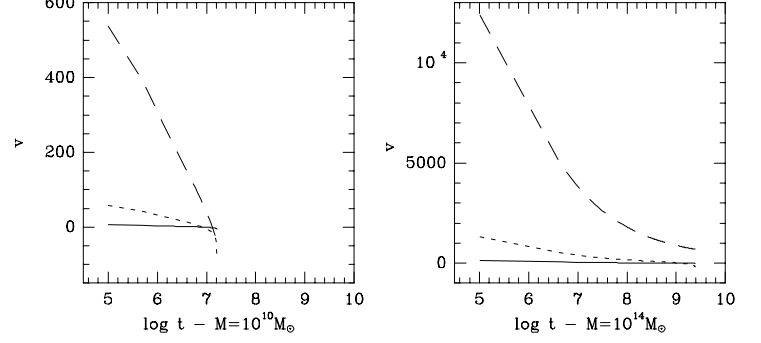
BARYONIC MATTER



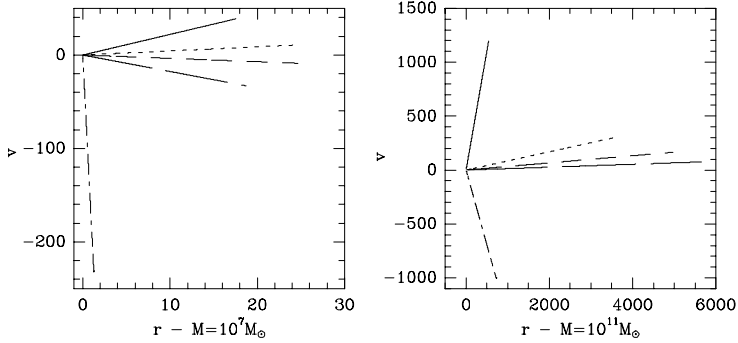
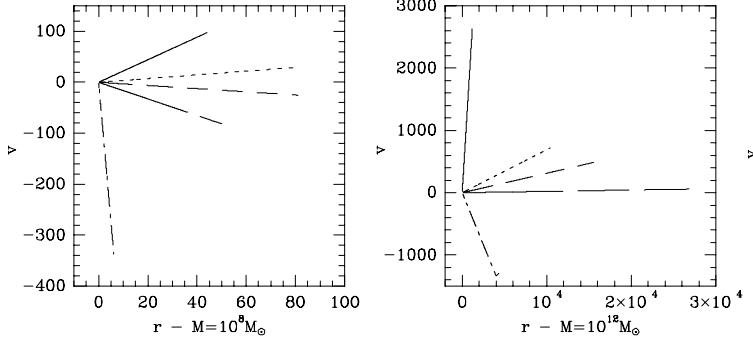
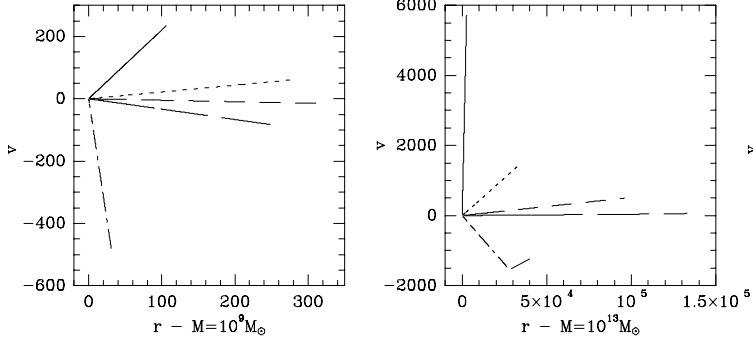
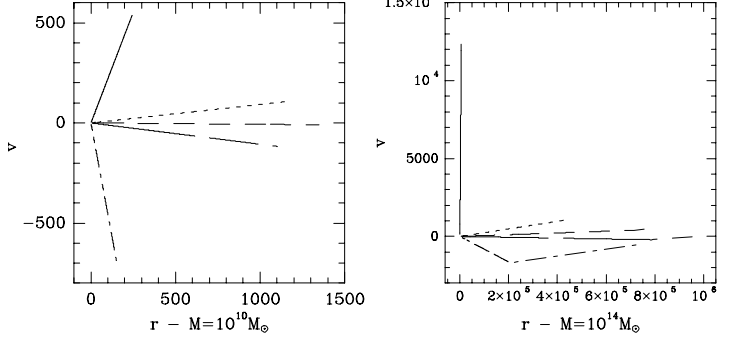
DARK MATTER



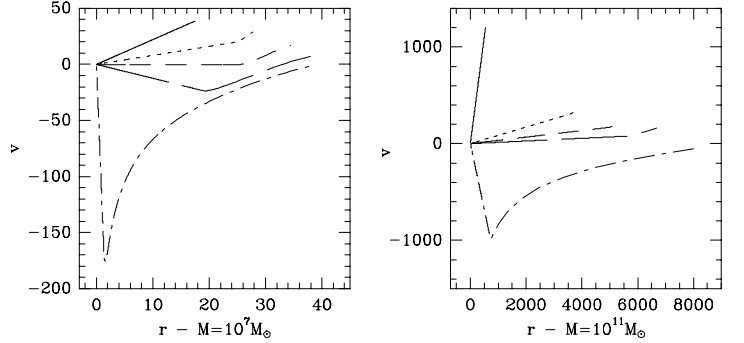
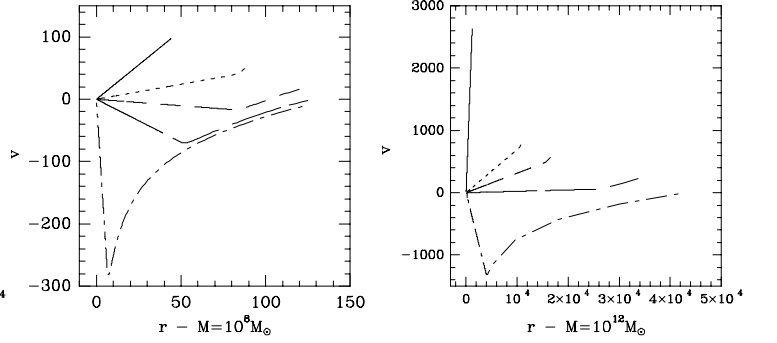
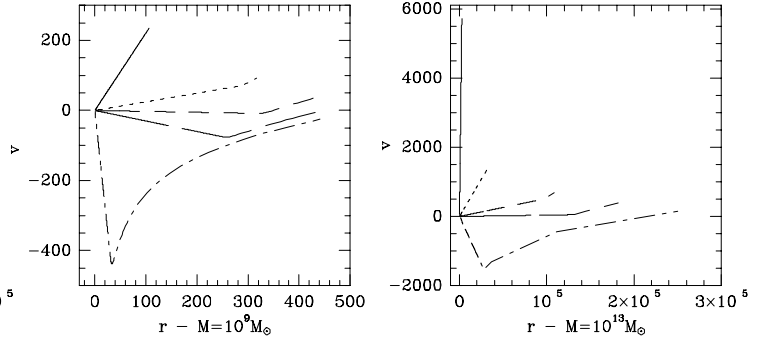
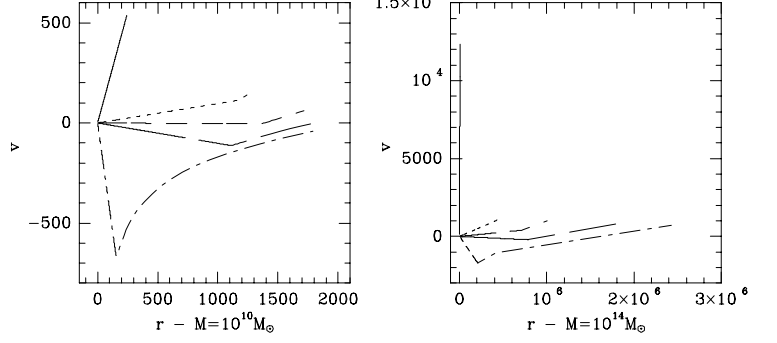
BARYONIC MATTER

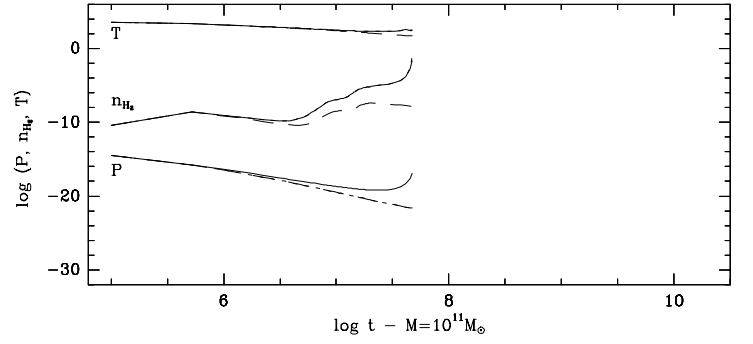
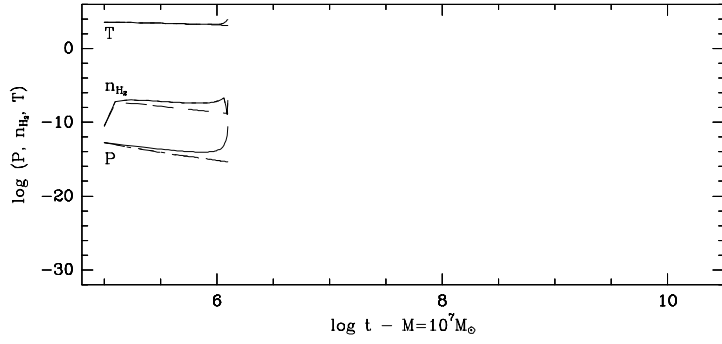
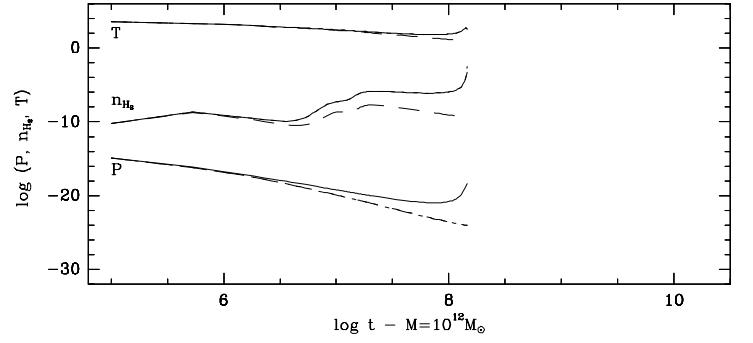
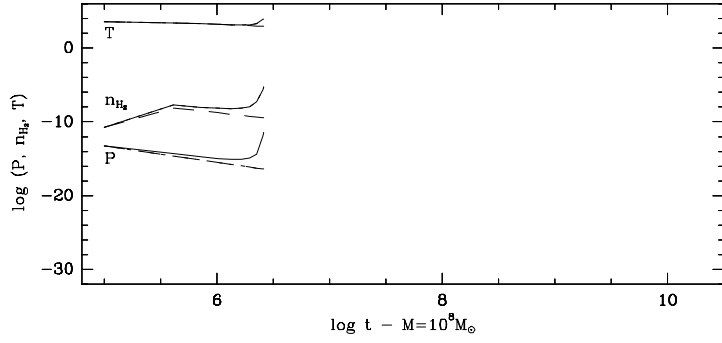
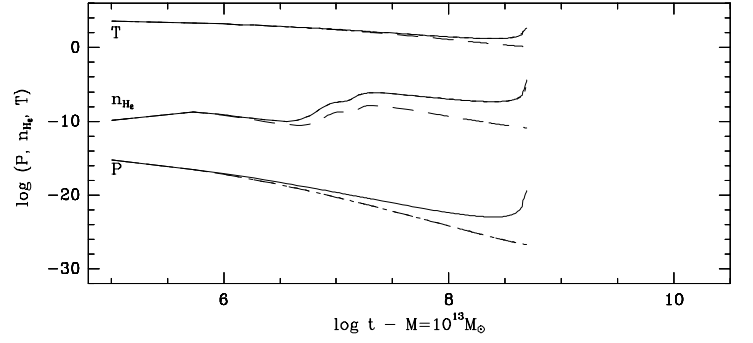
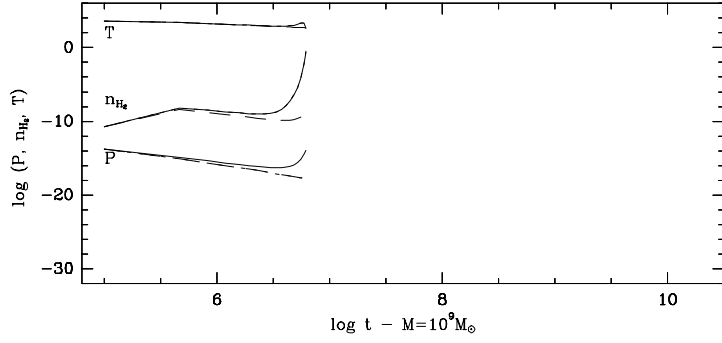
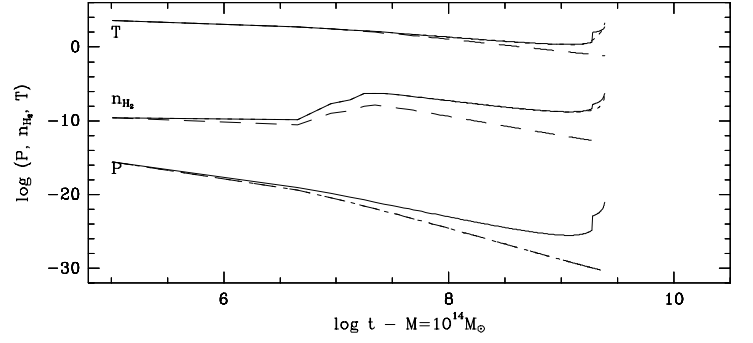
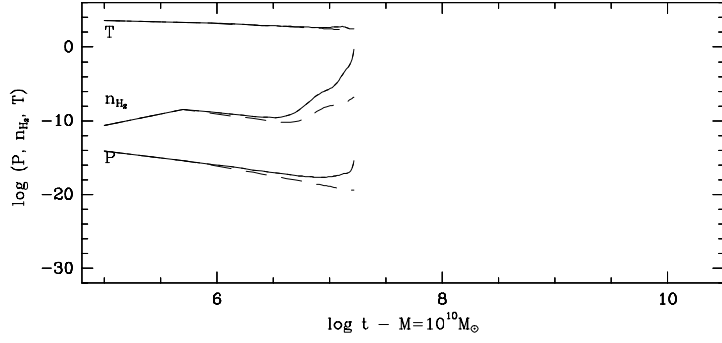


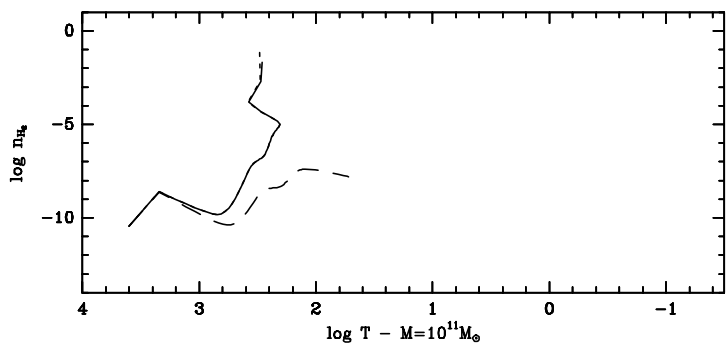
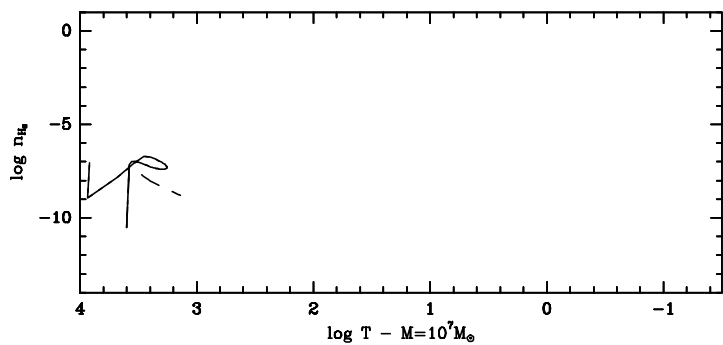
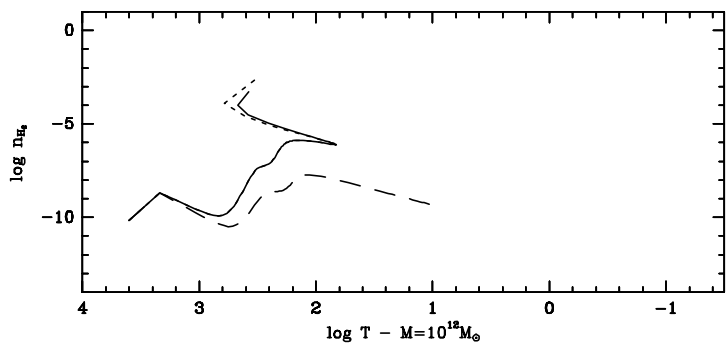
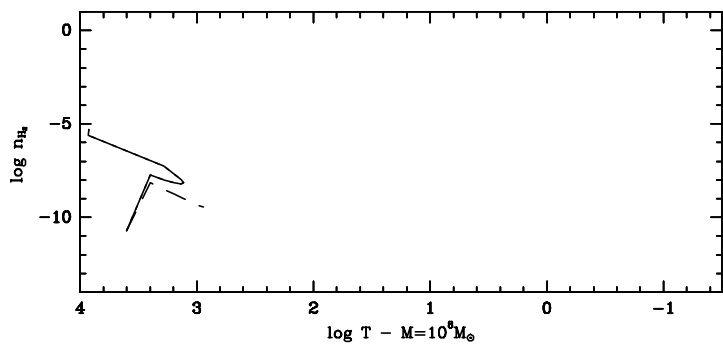
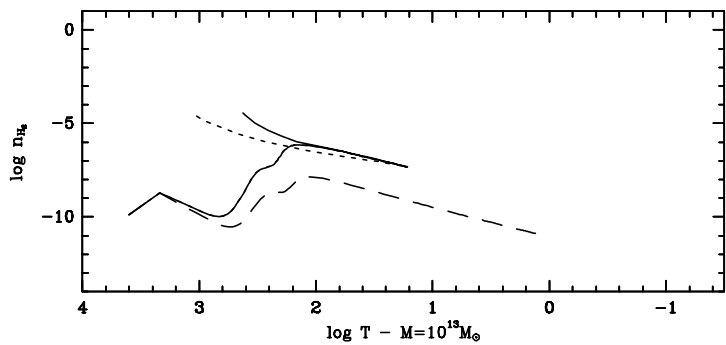
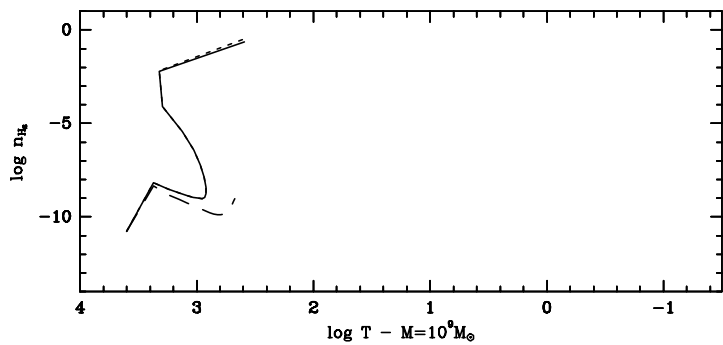
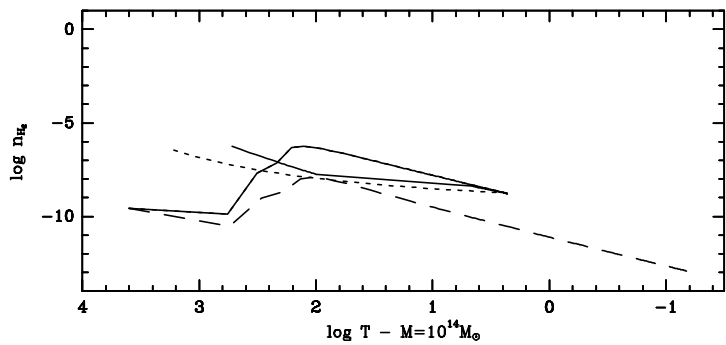
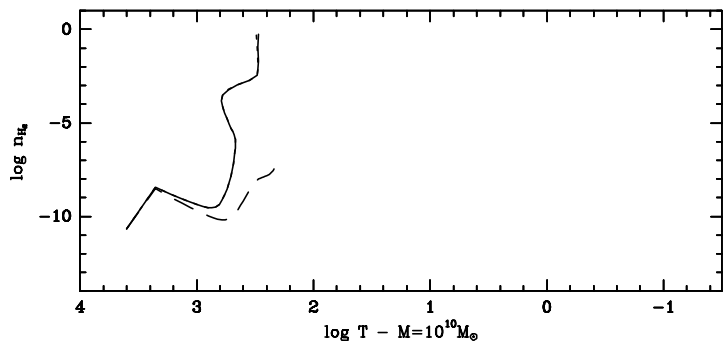
DARK MATTER



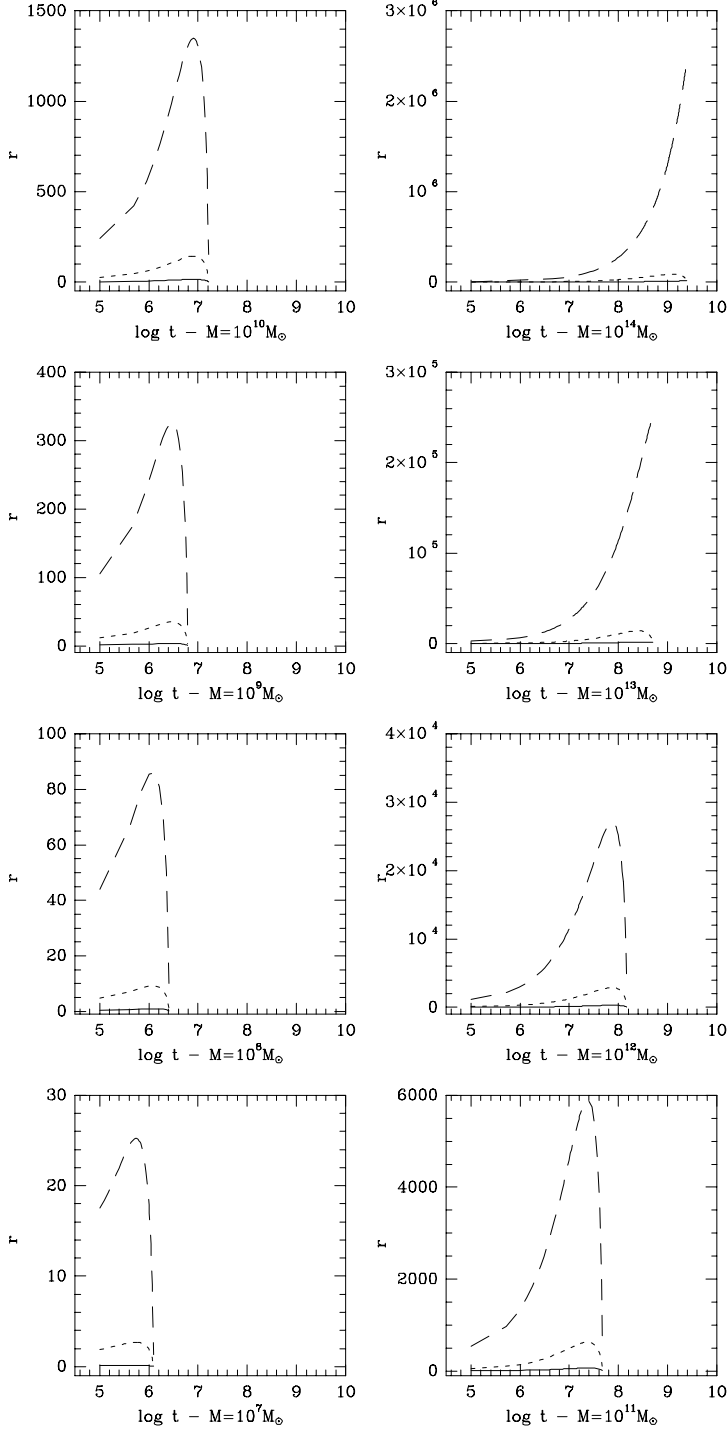
BARYONIC MATTER







DARK MATTER



BARYONIC MATTER

